Continuous Flow Paper Electrophoresis Miniaturization: Sickle Cell Hemoglobin Analysis

Yu-Hsuan Hsu

A thesis
submitted in partial fulfillment of
the requirements for the degree of

Master of Science

University of Washington
2025

Committee:
Barry Lutz
Paul Yager

Program Authorized to Offer Degree:
Bioengineering

University of Washington

Abstract

Continuous Flow Paper Electrophoresis Miniaturization: Sickle Cell Hemoglobin Analysis

Yu-Hsuan Hsu

Chair of the Supervisory Committee:

Barry Lutz

Bioengineering

Continuous flow paper electrophoresis (paper CFE) is a field separation technique utilized for the separation of various charged molecules. It is capable of processing any volume and serving as both an analytical and preparative tool. However, traditional paper CFE systems are limited by their large size, high power requirements, and long operation times, primarily suited for well-resourced laboratory settings. This project aims to address these limitations by miniaturizing paper CFE to a portable scale and reduce dependency on high voltage sources to expand the accessibility of electrophoresis separation. By changing the driven force from gravity in the traditional paper CFE to a capillary-driven system, and manipulating buffer composition, the project seeks to design a platform to achieve the separation of analytes. The project investigated the utility of the platform on detecting sickle cell hemoglobin as an analytical tool. Sickle cell hemoglobin results from a point mutation in the wild-type hemoglobin, altering a single amino acid in its structure, leading to different hydrophilicity and isoelectric point. The separation principle in this platform mainly depends on the difference in isoelectric point of the analytes. The successful development of this platform will provide a new tool contributing to improved disease management and patient outcomes. As the result, the designed prototype, with dimensions of approximately 4 cm*10 cm and operating at 30 V to 50 V, offers portability and reduced power requirements, and the separation of low molecular weight analytes and proteins was observed. Further work is needed to optimize the separation between proteins. The platform also shows potential for hemoglobin quantification. Overall, this project is a proof of feasibility and an advancement toward creating an analytic or preparative device that can be used in both basic lab settings and point-of-care tests in the field, making it more accessible outside of traditional labs.

TABLE OF CONTENTS

Acknowledgements

I extend my heartfelt gratitude to my PI, Dr. Barry Lutz, my committee member, Dr. Paul Yager, and my mentor, Enos Kline, whose guidance and support have been invaluable throughout this thesis project and made this work possible. I'm especially grateful to Dr. Lutz for the thoughtful feedback and guidance he provided during our meetings, which helped me navigate challenges and refine the vision of this project. I am also deeply thankful to Enos Kline for his dedicating time to sourcing materials, assisting in the creation of reference proteins, offering insightful ideas, and providing mentorship and training throughout both my undergraduate and master's journeys. Special thanks to Shane Gilligan-Steinberg for fabrication instrument training and the initial idea of paper CFE, to Rose Duong for her insights on binder strategies for future work, to Nello Gu for his advice on quantitative analysis, and to Garima Thakur for her helpful input during group meetings. I truly appreciate the generosity, encouragement, and helpful communication from everyone in the lab. Additionally, I want to thank my family for their support, and my dog Liala for keeping me company and reminding me to take breaks (and walks).

CH1 Clinical Background - Sickle Cell Disease

1.1 Sickle Cell Disease

Sickle cell disease (SCD) is an inherited red blood cell disorder associated with abnormal hemoglobin [1]. The abnormal hemoglobin reduces the ability of red blood cells to carry oxygen and distorts the cell shape. Sickle cells have shorter cellular life spans compared to normal red blood cells. They also have hard, sticky, sickle-shaped cell structures, leading to red blood cell shortage, clogged blood vessels, and damaged organs in the long term. In 2021, the global incidence of SCD in newborns was approximately 515,000, and people living with SCD were about 7.74 million, with a total mortality burden of around 385,000 [2]. From 2000 to 2021, the global total incidence and newborn incidence increased 41.4% and 13.7%, and the total death of people with SCD increased by 20.8%. SCD is prevalent in historically malaria-endemic regions, including sub-Saharan Africa, India, the Mediterranean, and the Middle East. This distribution is linked to the evolutionary advantage of the heterozygous genotype, which reduces the severity of malaria, whereas the homozygous genotype leads to disease [3]. In 2021, newborns with SCD in sub-Saharan African were estimated to be 405,000, which had increased by 27.2% from 2020, due to the population growth in that region. In the United States, it was estimated that about 100,000 people live with SCD [4]. The condition is most common among African Americans, occurring in about 1 in every 365 births in this population, while the incidence among Hispanic Americans is roughly 1 in 16,300 births. Additionally, around 1 in 13 African American newborns carries the sickle cell trait.

SCD is an autosomal recessive inheritable disease associated with a point mutation in *HBB* gene, which is the gene that code for the sickle cell hemoglobin (HbS) [5]. SCD symptoms occur

when an individual inherits genes of HbS from both parents (HbSS), or a combination of genes of HbS and other abnormal hemoglobin variants such as HbC or β-thalassemia (HbSC, HbSβ^0-thalassemia, HbSβ$^+$-thalassemia), where HbSC and HbSβ$^+$-thalassemia are the milder forms of SCD compared to HbSS. Sickle cell trait (SCT) occurs when an individual only inherits one copy of the HbS gene from a parent and inherits a copy of normal hemoglobin (HbA) from the other parent. People living with SCT do not exhibit SCD symptoms, but there is a risk of passing the HbS gene to their children, inducing the risk of the children having SCD. HbS results from a single DNA nucleotide base pair mutation in the 6th codon, GAG to GTG, on the β-globin gene, changing the amino acid glutamine to valine at that site [6]. The change of amino acid in HbS leads to a more hydrophobic structure and allows polymerization when deoxygenated. Although SCD is caused by a mutation in a single gene, the symptoms and severity of the disease are influenced by multiple genes. These genes, which do not directly encode the β-globin protein but modulate disease expression, are referred to as pleiotropic or modifier genes [5].

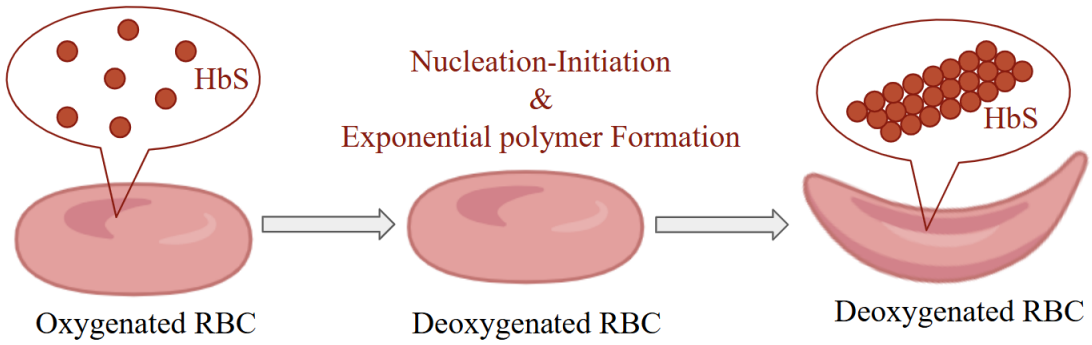

Figure 1: *Schematic of HbS polymerization in red blood cells (RBCs). (Created with BioRender.com)*

As mentioned earlier, the mutation in HbS allows it to undergo polymerization when deoxygenated, due to valine binding to the nearby globin chain [6]. The polymerization of HbS

also depends on factors such as HbS concentration, oxygen level, pH, and fetal hemoglobin (HbF) concentration. HbS polymerization is a nucleation-initiated process, meaning it requires an initial step of nucleus formation, leading to a delay period before the polymerization begins. Once the nuclei are formed, the polymer grows exponentially, forming rope-like fibers that distort the red blood cell into the sickle shape (*Figure 1*). This distortion disrupts blood flow through microvasculature and leading to vaso-occlusive crisis, also known as sickle cell crisis, which the most common manifestation of SCD [7]. It is caused by a complicated mechanism involving trapping of sickle cells in microvasculature, worsened by the adhesion of erythrocytes to the endothelium, the aggregation of leukocytes and sickled cells, and inflammation from neutrophil transmigration. Vaso-occlusive crisis leads to severe pain in patients because blood flow is blocked, preventing oxygen and nutrients from reaching tissues. This causes tissue damage and inflammation, which will trigger pain. Other complications of SCD include vitamin deficiency, delayed growth, joint problems, blood clots, acute chest syndrome, enlarged spleen, sickle retinopathy, aplastic crisis, splenic sequestration crises, etc. [8]. Additionally, HbF is the major form of hemoglobin during fetal development. In healthy individuals, it will gradually be replaced by HbA, the wild-type hemoglobin, after birth. However, in individuals with SCD, it will be replaced by HbS instead of HbA [9]. Newborns with SCD typically do not exhibit symptoms until their HbF level decrease to the adult level, usually around by 5 to 6 months after birth, since a higher concentration of HbF in the blood can help prevent HbS polymerization [10]. As a result, early diagnosis is critical before symptoms emerge, enabling timely interventions that can significantly improve clinical outcomes.

1.2 Current Treatments

The treatments of SCD are divided into two major categories: (1) disease-modifying therapies, and (2) curative treatments.

Disease-modifying Therapies

One of the disease-modifying therapies is hydroxyurea. It works by increasing the concentration of HbF through inhibition of ribonucleotide reductase, which resulting in the gene expression of γ-globin for HbF instead of the β-globin of HbS [9], [11]. Studies showed that hydroxyurea treatment reduces the vaso-occlusive crisis by 44% and leads to fewer episodes of acute chest syndrome, which is a common complication of SCD that is characterized by pulmonary infiltrates [9], [12]. It was approved for use in adults in 1998 and for children ⩾ two years old in 2017 by the US FDA. Additionally, the BABT HUG study showed that hydroxyurea is safe in infants [9]. Therefore, in 2014, it was recommended to offer hydroxyurea to all infants ⩾ 9 months with HbSS or HbSβ^0-thalassemia even if they have not yet shown symptoms. Hydroxyurea is typically safe and causes few permanent side effects, but myelosuppression is one adverse effect that can have a significant impact, which is a condition where the bone marrow cannot produce blood cells properly [13]. Therefore, close laboratory monitoring is needed after hydroxyurea administration. Additionally, effective hydroxyurea treatment requires good adherence and consistent use over several months for it to work [9]. Although hydroxyurea is a standard treatment for preventing vaso-occlusive crisis, the accessibility and affordability in low- and middle- income counties are low [14].

Another disease-modifying therapy is transfusion therapy, which involves receiving or replacing blood [9]. The rationale behind this therapy is to decrease the concentration of HbS in

the blood. There are three kinds of transfusion therapy. First, simple transfusion involves giving the individual blood containing HbA without removing their own blood. However, since no blood is removed, it is important to ensure that the total hemoglobin concentration does not become too high after transfusion, as this can lead to increased blood viscosity and induce complications like hypertension and cerebral hemorrhage. The second type is partial manual exchange transfusion, where a certain amount of the patient's blood is removed through phlebotomy before receiving healthy blood. This method helps reduce the risk of blood becoming too viscous. The third one is automated red cell exchange transfusion. This method utilizes a specialized instrument to continuously exchange patient's blood with healthy blood, which is the most efficient and effective way to reduce HbS concentration among the three methods. However, having a safe blood supply is the greatest challenge to doing blood transfusion for SCS in low resource settings. Recommended practices for blood transfusion from WHO have not yet been fully adopted in sub-Saharan Africa [14]. According to WHO, the average blood donation rate in high-income countries is three times higher than in African countries. Additionally, the majority of hospitals do not have access to equipment for automated red cell exchange transfusion and only half of the hospitals in Nigeria are able to perform simple transfusion or partial manual exchange transfusion [14].

Administration of L-Glutamine is another disease-modifying therapy that is the first oral medication approved for SCD by FDA. It works by increasing the level of nicotinamide adenine dinucleotide (NAD+) to prevent oxidative damage to the red blood cells, since L-glutamine is a precursor for NAD+ synthesis [9]. Studies showed that children with SCD have 47% lower glutamine levels. A study showed that with the administration of L-glutamine, the number of cases with vaso-occlusion crisis was reduced by 25%. The common side effects of L-glutamine are generally gastrointestinal side effects like nausea, abdominal pain, or constipation. However, L-

glutamine is not approved by the European Medicines Agency since the efficacy is considered not sufficient [14].

Curative Treatments

On the other hand, curative treatments refer to treatments that can completely cure SCD. Currently, hematopoietic stem cell transplantation (HSCT) is the only treatment capable of curing SCD [9]. HSCT, also known as bone marrow transplantation, involves transplanting healthy hematopoietic stem cells to the patient [15]. These stem cells can differentiate and proliferate into various types of blood cells, allowing the patient to produce healthy blood cells on their own using the transplanted stem cells. With a matched sibling donor, which less than 20% individual with SCD have, the overall survival rate has been 93%-97% and the disease-free survival rates are 82%-100% after receiving HSCT [9]. With matched unrelated donors or haploidentical donors, the rate of graft-versus-host disease is higher and has led to mortality. This approach is still under investigation and is not yet considered standard treatment. Despite its ability to cure SCD, HSCT is not available in sub-Saharan Africa and is already limited to the small number of patients who have a matched sibling donor [14].

In recent years, there has been a growing interest in gene therapy research. Since SCD is caused by a point mutation in a single gene, gene therapy has been considered a highly promising curative treatment. The first successful case of gene therapy in SCD was reported in 2017 [9]. Casgevy and Lyfgenia are the first two gene therapies for SCD approved by the FDA in 2023 [16]. Casgevy is also the first FDA approved CRISPR/Cas9 gene therapy. It works by targeting the BCL11A gene in the hematopoietic stem and progenitor cells, leading to the increased production of HbF [17]. On the other hand, Lyfgenia used a lentiviral vector to correct the mutation in the stem cell, enabling the individual that received Lyfgenia to produce HbA instead of HbS [16]. After

gene modification, the stem cells are transplanted back into the patient. Since the stem cells are autologous, there is a reduced risk of graft-versus-host disease compared to HSCT.

1.3 Current Diagnostic Methods

Key measurements for SCD diagnostics include the identification and quantification of hemoglobin variants. These measurements help differentiate between trait and disease, assess severity, and monitor treatment. The hemoglobin variants relevant for SCD diagnostics include HbS, HbA, and HbC [18]. Quantifying these variants allows differentiation between trait and disease by determining the relative amounts of HbS/HbC to HbA, which also provides insight into disease severity. Additionally, the amount of HbA is important for distinguishing between HbSS and HbSβ^+ [19]. For treatment monitoring, many therapies aim to decrease HbS levels or increase HbA or HbF levels. Therefore, quantification enables clinicians to evaluate whether these levels have shifted toward effective therapeutic concentrations.

Traditional SCD Diagnostic Methods

SCD is diagnosed by detecting the presence of HbS. It was predicted that low-cost screening and consequent treatments could prevent 70% of early SCD-related mortalities [20]. However, the traditional SCD diagnostic methods that were commonly used are mostly cost- or time-intensive. One of the methods is hemoglobin electrophoresis, which is recommended by WHO for SCD diagnosis [21]. Studies have shown that different hemoglobin variants have varied electrophoretic mobilities under electrophoretic separation [22].

Hemoglobin electrophoresis separates hemoglobin variants based on their electrophoretic mobilities in an electric field. There are two common ways to perform hemoglobin electrophoresis to diagnose SCD: cellulose acetate electrophoresis at alkaline pH and citrate agar electrophoresis

at acidic pH [23]. Cellulose acetate electrophoresis at alkaline pH separated hemoglobin variants by their difference in electrophoretic mobility. At alkaline pH, the hemoglobin will possess negative charges and migrate toward the positive electrode differently based on their different in charge properties. This method provides rapid separation and is easy to perform. However, it utilizes high voltage, 250 V-300 V [24]. High concentrations of HbF reduce the overall HbS concentration in the blood, making HbS signals more likely to be missed. Citrate agar electrophoresis at acidic pH is good at separating HbS from HbA even in the presence of abundant HbF utilizing the interaction of the agaropectin in the gel with Hb variants [25]. However, the method is technically difficult. It requires stricter temperature control since the electrophoresis runs at 4°C. Both hemoglobin electrophoresis methods produce relatively wide bands, which can lead to the overlap of multiple hemoglobin variants. When HbF is present at high concentrations, it often forms a broad band that overlaps with other hemoglobin variants of interest, making identification more difficult.

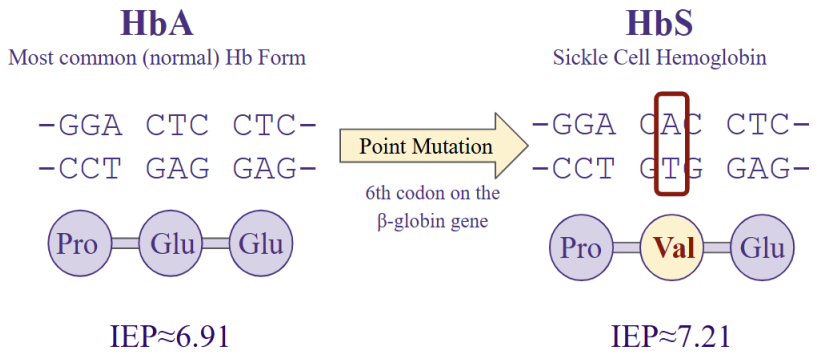

***Figure 2**: Sickle cell hemoglobin mutation.*

Another common method of SCD diagnostics is isoelectric focusing. Mutation of hemoglobin proteins leads to change in their isoelectric points (IEP). IEP is defined as the pH value at which the protein has no net electrical charge. In a previous study, the IEP of HbA was estimated

to be 6.91, while the IEP of HbS was estimated to be 7.21 (*Figure 2*) [26]. Isoelectric focusing is a type of electrophoresis that separates the analytes based on their IEP [27]. By applying an electric field over a medium with a pH gradient, the analytes will tend to be focused at the location with pH corresponding to their IEP. Isoelectric focusing produces finer bands and provides higher spatial resolution compared to hemoglobin electrophoresis. The downside of this method is that it requires even higher voltages than hemoglobin electrophoresis--1000V or more. It is less quantitative than high-performance liquid chromatography and requires skilled interpretation due to the high number of bands [25].

High-performance liquid chromatography (HPLC) is another commonly used SCD diagnostic method, especially for newborn screening [28]. When hemoglobin variants are forced through an ionic exchange column (stationary phase) under pressure using phosphate buffers of varying concentrations (mobile phase), they exhibit distinct retention times due to their differential interactions with the stationary phase. The separation of hemoglobin variants based on the retention time allows more accurate quantification of the analytes. However, the disadvantage of HPLC is the high cost. The HPLC instrument and the analyzing software are expensive, and the column needs to be replaced regularly since the column quality will affect HPLC performance. The HPLC instruments are also large, heavy, complex, and delicate, which makes it hard to perform HPLC outside of a laboratory setting.

The diagnostic methods introduced above (electrophoresis, isoelectric focusing, HPLC) all require laboratory processing and have long turnaround times. However, in low-resource settings, laboratories and trained personnel are often limited, and shorter turnaround time is desired to enable timely diagnosis and treatment and to improve patient outcome[14].

There is a low-cost and fast test SCD detection method called sickle solubility test (SST), which utilizes the difference in solubility to detect HbS. HbS is less soluble when deoxygenated compared to other hemoglobin variants. When HbS is present, HbS precipitates and the solution becomes opaque. The benefit of this method is that it is cheap and provides a rapid screen that takes about 10 minutes. However, the limitation is that it can only detect the presence of HbS, so it is unable to distinguish SCT and SCD, and it has a high rate of false positive and false negative results [14] [29].

Point-of-care Diagnostic Method for SCD

Due to the limitations of the traditional diagnostic method for SCD in low resource setting, several point-of-care (POC) testing methods have been developed, such as the Gazelle Hb Variant test, HemoTypeSC, and SickleSCAN; these are three currently-commercial-available POC tests for SCD [14] [30].

The Gazelle Hb Variant test is the commercial version of a POC test optimized from HemeChip, which was originally developed in 2013 by the Gurkan group [31]. It is a POC micro-chip test that separates hemoglobin variants based on their differences in electrophoretic mobility, which depends on their mass-to-charge ratio, similar to conventional hemoglobin electrophoresis [32]. The device uses single-use disposable cartridges that contain cellulose acetate paper, where the separation of hemoglobin occurs, and stainless-steel electrodes. The other main component is a portable, automated reader with rechargeable power source that supplies power for electrophoresis, performs real time imaging of hemoglobin separation, and analyzes the peak positions for relative quantitative interpretation [33]. The procedure involves first obtaining a whole blood sample with finger prick [31]. The sample is then diluted and lysed before being loaded onto the microchip. After that, the microchip is inserted into the reader. It then starts

performing electrophoresis by applying an electric field across the cartridge, capturing real-time images, and analyzing results. The procedure takes approximately 10 minutes. With the multispectral reading technique, Gazelle Hb Variant can distinguish HbA, HbF, HbS, and HbC. However, it is not able to differentiate between HbC, HbE, and HbA2, since these variants migrate to a similar location during electrophoresis. HbE is a hemoglobin variant caused by point mutation in the beta-globin gene [34]. Individuals with HbE trait typically have no symptoms or only mild anemia, and it is not considered a form of SCD. HbA2 is a normal hemoglobin variant composed of two alpha and two delta globin chains, whereas HbA contain two alpha and two beta globin [35]. The inability to distinguish HbC, HbE, and HbA2 may lead to false-positive results and misinterpretation during screening. The Gazelle Hb Variant test received regulatory approval from nine countries in 2021 and is currently available in those countries, primarily in Africa [31]. Although it offers high accuracy and quantitative analysis as a POC device, one of its greatest limitations is the high manufacturing cost. While the estimated cost per test is around $2 to $2.5 USD, the instrument itself is priced between $1,200 to $1,500 USD [32]. Although this is significantly lower in both cost and turnaround time compared to conventional hemoglobin electrophoresis and HPLC, it is still considered expensive and limits widespread use in low-resource settings.

HemoTypeSC is another POC test for detecting hemoglobin variants. HemotypeSC is a lateral flow test that uses monoclonal antibodies to capture specific hemoglobin variants. The test strip contains four lines, each with immobilized antibodies specific to different hemoglobin variants: (1) a control line that captures all hemoglobin types, (2) a line for HbA, (3) a line for HbS, and (4) a line for HbC [18]. Between 1uL to 15uL of whole blood is diluted in 1mL of water to lyse the red blood cells, and the HemoTypeSC strip is dipped into the solution. As the sample

flows through the strip, hemoglobin and gold nanoparticles compete to bind to the antibodies immobilized on the strip. If the target hemoglobin is present, it binds to the antibody first, blocking the gold nanoparticle, and the line will not appear. If the hemoglobin variant is absent, the gold nanoparticle binds to the antibody, producing a visible red line. The entire process takes about 20 minutes and is readable by eye, requiring no instrument or power. Studies show that HemoTypeSC reaches 99.1% accuracy, with a sensitivity of 93.1% and specificity of 99.9% for HbSS [36]. It was estimated that the cost of material per strip is less than $0.25 USD, and the strips remain stable at 40°C for over 2 years [18]. This method can only detect hemoglobin variants for which a specific capture antibody has been immobilized on the test strip. This targeted approach enhances specificity to detect Hb variants that are relevant to SCD. As a result, the test is not affected by high concentrations of HbF, which commonly interfere with other detection methods. The study also showed less than 0.1% of cross-reactivity between antibodies and the non-target variants. However, it does not provide quantitative results, which is important for distinguishing HbSβ^+-thalassemia from sickle cell trait [18]. Additionally, the result interpretation is counterintuitive. Unlike most tests where visible line indicates a positive result, HemoTypeSC shows positive result with the absence of line. Therefore, if the person is not properly trained, there is a risk of misinterpreting the results.

SickleSCAN is also a lateral flow assay designed to detect hemoglobin variants. Unlike HemoTypeSC, which is a competitive lateral flow assay, SickleSCAN uses a sandwich lateral flow assay. The test strip also contains four lines: a control, and lines for HbS, HbC, and HbA [19]. Using a capillary sampler, 5uL of whole blood is obtained via finger prick, mixed with a hemoglobin solubility buffer, and then applied to the sample port on the strip. As the solution flows, the respective hemoglobin variants bind to their corresponding lines. To visualize the result, a

colorimetric method is used: blue nanoparticle-conjugated antibodies that can bind to all types of hemoglobin via the α-globin chain are used. A positive result appears as a blue line on the strip, which aligns with standard (intuitive) test interpretation. The entire procedure, from sample collection to result interpretation, takes less than 10 minutes, while the lateral flow strip itself produces visible results within approximately 2 minutes after sample application. The sensitivity and specificity for detecting HbSS, HbAS, HbSC, HbAC, and HbAA are all reported to be above 99%. The limit of detection (LoD) differs among hemoglobin variants: 40% for HbA, 1% for HbS, and 2% for HbC, measured as a percentage of total hemoglobin. This is an intentional design feature so that $HbS\beta^+$ can still be recognized as SCD by the showing the HbS line, though the test cannot distinguish between HbSS and $HbS\beta^+$ due to the lack of quantification ability since the intensity of the line does not reflect the hemoglobin concentration. The low LoD for HbS is clinically sufficient, as individuals with SCD typically exhibit HbS levels well above 1%. The study also reported that the result is not affected by up to 30% HbF, which is common in individuals treated with hydroxyurea. However, since infants may have up to 90% of HbF levels, further validation in newborn clinical setting is recommended [32]. The cost of SickleScan is higher than that of HemoTypeSC, but is still estimated to be lower than $5 USD [30].

1.4 Clinical Gap and Project Motivation

Over 80% of newborns with SCD are born in sub-Saharan Africa [14]. However, the mortality rate of SCD in sub-Saharan Africa is much higher than that in high-income settings. Studies have shown that the under-five mortality rate of SCD is high in low- and middle- income counties. For example, in sub-Saharan Africa, the under-five mortality rate of SCD is about 50%, whereas in the high-income settings, 94% of individuals with SCD survive into adulthood. This disparity is largely due to the low accessibility to diagnostics methods and treatments. With early

diagnosis, newborns can begin penicillin or hydroxyurea treatment to reduce the risk of infection from pneumococcal sepsis or the development of sickle cell crisis [14], [37]. The mortality from pneumococcal sepsis has been found in children with SCD to be 20%. Studies show that early penicillin is associated with 84% reduction in infection. Moreover, pregnancy termination remains inaccessible or restricted for many women. Therefore, accessible diagnostic tools that allow parents to determine whether they are HbS carriers can support informed reproductive decisions and help reduce the burden of SCD. Although POC test had been developed to detect SCD hemoglobin variants, current options have limitations. Quantitative tests are more expensive, while the lateral flow assays are cheap but only provide qualitative results. However, quantitative results are important for monitoring disease severity, differentiating between traits and disease, tracking treatment response, etc. This thesis aims to address these limitations by developing a simplified, low-cost POC device designed for decentralized screening of SCD in low resource settings. The device focuses on miniaturizing continuous-flow paper electrophoresis (paper CFE), offering the potential for greater accessibility and field usability.

CH2 Technical Background-Continuous Flow Paper Electrophoresis

2.1 Continuous Flow Paper Electrophoresis

Continuous flow electrophoresis (CFE) is a field separation technique that has been applied to fractionate various samples based on differences in charge and electrophoretic mobility. It works by separating charged biomolecules or particles as they flow through a chamber under an applied electric field (*Figure 3*). CFE allows continuous sample input and real-time separation. This enables processing large sample volumes while maintaining biological activity, achieving high sample recovery, and supporting real-time collection of multiple separated components. Various electrophoretic modes have been established, with different separation principles and device design [38]. For example, zone electrophoresis (ZE) separates based on the charge-to-mass ratio, isoelectric focusing (IEF) separates amphoteric molecules by their IEP, isotachophoresis (ITP) utilizes leading and trailing electrolytes to form focused analyte zones based on their relative electrophoretic mobility, and field step electrophoresis (FSE) utilizes differences in buffer conductivity to create regions of varying electric field strength and separate analytes faster at the center zone [39]. In terms of device design, common formats include rectangular bed, trapezoidal bed, void channel devices, and chip-based miniaturized devices [38]. CFE has been applied to the separation and fractionation of samples containing proteins, peptides, DNA, organelles, extracellular vesicles, and other biomolecules.

Paper CFE is a type of CFE that uses a paper substrate as the separation medium. The use of paper offers advantages such as low cost, ease of fabrication, and suitability for low-resource settings. In paper CFE, the sample is introduced into a continuous flow of buffer through the paper medium. Electrodes are places across the paper to generate an electric field perpendicular to the

direction of the fluid flow. As a result, charged analytes are deflected toward either the positive or negative electrode, allowing spatial separation based on their electrophoretic mobility.

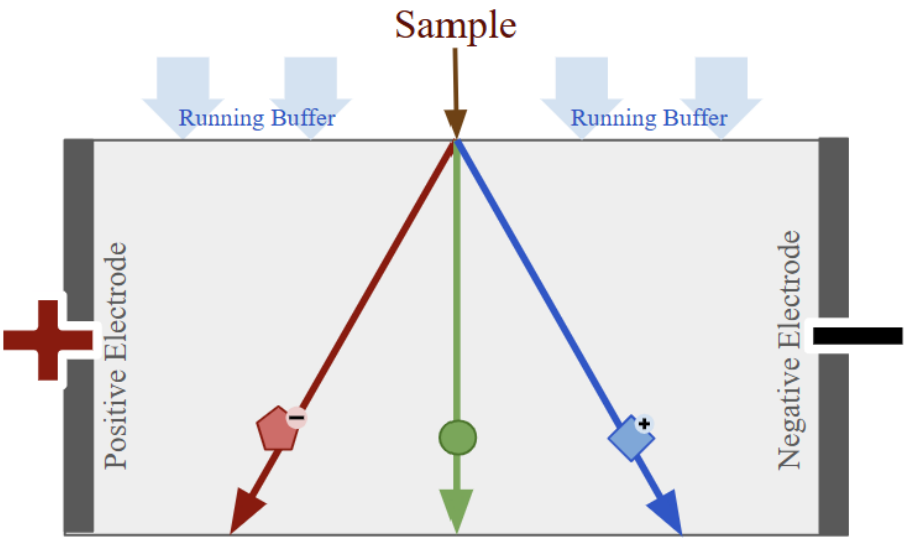

Figure 3: *Schematic illustration of continuous-flow electrophoresis (CFE).*

2.2 Development of Continuous Flow Paper Electrophoresis

The development of paper CFE traces back to the early 19th century. The peak of interest among researchers in studying paper CFE was during the 1950s. The two-dimensional paper-based electrophoresis served as an enhancement strategy to improve the resolution for separating analytes compared to one-dimensional partition chromatography. The concept of paper CFE was first introduced and attempted by J. ST. L. Philpo in 1940 [40]. In 1949, Svensson and Brattsen established an integrated paper CFE apparatus as continuous electrophoretic separation in flowing liquid utilizing gravity as the driving force [41]. The apparatus they established contained a buffer reservoir and multiple collection tubes at different heights. A filter paper was connected to the buffer reservoir and hung down to the collection tubes, allowing the fluid to flow from the reservoir

to the collection tubes under the influence of gravity. The electric field was exerted across the filter paper with the direction orthogonal to gravity by electrodes applied onto the filter paper. This led to the deflection of charged particles toward either electrode as they migrated down the filter paper. The bottom of the filter paper was designed as a jagged shape so the separated sample at different locations could drip down from different tips to the collection tubes to achieve sample recovery. Various analytes have been applied to this system, such as human salivary secretions, plasma, amino acid and protein mixtures, etc. [42] [43] [44]. It has been a useful tool to learn the chemical characteristics of analytes, fractionate complex biological fluids, and characterize pathological conditions, etc. And it was regarded as an efficient method for isolating and purifying single species from a complex matrix. Numerous researchers have explored various refinements to the techniques, including enhancements to the electrode system, optimization of cooling methods, and improvements in sample loading methodologies [42] [45]. The strengths of CFE include its ability to accommodate varying sample volumes and simultaneously collect or analyze multiple separated analytes. Traditional paper CFE systems employed filter papers exceeding or approximately 60 cm*60 cm in size and utilized voltages from 600V to 1000V. Moreover, the operation times extended for hours. These elements made it suitable for laboratory setups with more resources and stationary space for the apparatus. However, there exists an opportunity for improvement through miniaturization. By downsizing paper CFE systems to portable scales and reducing the power needed while preserving their capability in species separation within complex matrices, the potential arises for their integration as useful analytical or preparative tools in simpler laboratory setup or POC applications in lower resource settings.

In recent years, many studies on paper CFE have been conducted by the Šlais group. They utilized the principles of paper CFE and optimized the paper geometry, investigated the buffer

system configurations, and eventually developed a platform called divergent flow isoelectric focusing (DF-IEF) [46]. In traditional rectangular separation beds, a higher voltage drop is required to maintain separation resolution due to the trade-off between bed width and electric field strength. To address this limitation, the Šlais group introduced DF-IEF, which employs a trapezoidal separation bed, where fluid flows from a narrower inlet toward a wider outlet. This design allows analytes to be quickly separated under stronger field at the inlet, since with a fixed voltage drop, field strength decreases with distance.

$$E = \frac{V}{d}$$

E = Electric Field Strength; V = Potential Difference; d = Distance

As the fluid flows toward the wider outlet, the distance between the separated peaks increases proportionally with the expanding bed width due to the divergent flow. This geometry enables lower power needed while achieving comparable separation to that of a rectangular separation bed. They demonstrated successful separation of complex protein mixtures such as barley grain, malt, and beer, as a purification step before mass spectrometry analysis [47]. They also investigated buffer system compositions to eliminate the need for expensive carrier ampholytes, which are typically used to establish pH gradient for IEF [48]. The system operated at 700 V-800 V across a separation bed approximately 8 cm (outlet) by 15cm (bed length) in size, with an 8 cm height difference at the outlet. The total running time was approximately 30-40 minutes. This platform improved separation performance and reduced the size of paper CFE compared to the traditional CFE. However, the setup is still not suitable for POC application due to the high voltage requirement and the need for a height difference to drive the fluid flow by gravity and tubing in the inlet.

In terms of miniaturization, researchers have implemented CFE into micro scaled chip-based devices [38]. However, this thesis focuses on paper-based CFE, as we aim to avoid the need for precise pumps and tubing, which could reduce the accessibility of the device. Additionally, under high-voltage, bubble formation becomes an issue in micro scale separation channels due to electrolysis, which disturbs the system [49].

2.3 Project Overview

Hypothesis

Capillary-driven flow combined with optimized buffer composition can enable effective separation of proteins (HbA and HbS) on a miniaturized continuous flow paper CFE platform without the need for high voltage.

Rationale

This project used two strategies: capillary driven flow for miniaturization, and buffer design of electrophoresis for protein separation.

- Miniaturization strategy: Capillary Driven Flow

  The traditional paper CFE relies on gravity as the driving force of fluid, requiring vertical paper orientation and a height difference between the buffer reservoir and collection tube. This limits its potential for downsizing. This thesis proposes a miniaturizing strategy by shifting the gravity-driven system to a capillary-driven system, achieved through manipulation of paper materials with varying pore sizes and geometry and the incorporation of an absorbent pad at the flow endpoint. These modifications provide control over flow direction and rate, enhancing the potential for scaling down and the adaptability of the device.

- Separation strategy: Buffer System for Electrophoresis

  Proteins carry different net charges depending on the pH of the environment relative to their isoelectric point. By adjusting pH and applying an electric field, proteins with different isoelectric points can be directed in different paths and separated across the separation bed.

Goal

The goal of this project is to design and test a low cost, paper-based, continuous flow electrophoresis platform that can separate proteins based on their isoelectric points, with a focus on detecting and separating hemoglobin variants (HbA and HbS).

Project Overview

This project involves designing a paper CFE platform, selecting appropriate materials, optimizing buffer and pH conditions, and testing the platform using colored dyes, colored proteins and hemoglobin samples. The process includes building the physical device, identifying conditions that allow clear separation, and analyzing how different factors such as pH stability, salt concentration, and paper surface properties affect performance. The final goal is to miniaturize the technique of paper CFE and evaluate whether this system can be developed into a practical diagnostic tool and what improvements are needed to make it reliable for real-world use. If successful, this platform could serve as proof of feasibility in developing a diagnostic tool for SCD in low resource setting with miniaturized paper CFE.

CH3 Platform Prototype Development

3.1 Capillary Driven Flow

Capillary pressure is a physical phenomenon that arises at the liquid-air interface and creates negative pressure [50]. It depends on surface tension, channel size, and the contact angle of the liquid as described in Young-Laplace equation [51]. In porous media like paper, it can be used to drive flow without external pumps. Materials with larger pore sizes exhibit a lower magnitude (less negative) capillary pressure, whereas smaller pores generate higher magnitude (more negative) capillary pressure. A larger capillary pressure corresponds to a stronger driving force for fluid uptake and a greater tendency to retain the absorbed fluid. Consequently, fluid tends to migrate from regions of lower magnitude capillary pressure (larger pores) to higher magnitude capillary pressure (smaller pores). At the microscale, capillary forces can exceed gravitational forces, allowing control of fluid flow direction regardless of gravity. In this project, we utilize capillary pressure to direct flow for CFE instead of utilizing gravity by implementing a pore size gradient from large to small and selecting appropriate materials. This approach enables control over both flow direction and rate, supporting the development of portable, pump-free POC diagnostic systems.

3.2 Paper material selection

The paper material used for the separation bed is important because it must serve as a suitable medium for separation without interfering with the analytes, while also supporting the desired paper geometry. The key properties include high thermal tolerance, desired flow rate, minimal dispersion, and low protein adhesion. To select a suitable paper material, a flow test was conducted using bovine hemoglobin (bovine Hb) on 6-cm-long strips made from different types

of paper. Bovine Hb was chosen because the target analyte in the system is human Hb, and bovine Hb serves as a good model while avoiding the need for a BSL-2 setup at this stage. The running buffer used here is 1x TBE (pH 8.4), which is the buffer that HemeChip used in their electrophoresis for sickle cell hemoglobin. The flow patterns of bovine Hb were recorded and observed over time for comparison. (Note: In this thesis, the material used for separation bed was also refer to as "testing paper").

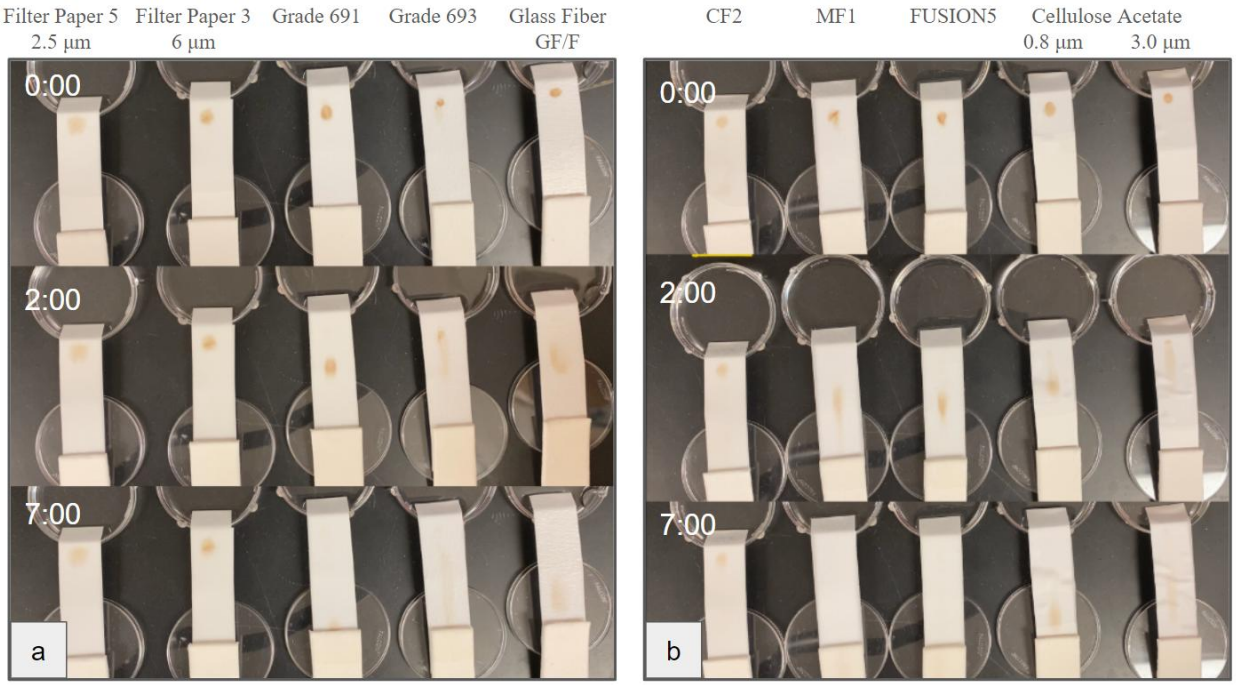

Figure 4: *0.1x Bovine Hb (15 g/L) flow pattern on different paper materials. The figure shows the images captured at three time points (0:00, 2:00, and 7:00 minutes) within the 20-minute video. Five papers were tested and recorded at a time, which is shown in the figure as (a) and (b). Sample was loaded on each paper with a 10 second interval from left to right. The 0:00 started counting as the last sample was loaded on the right-most paper in each video (GF/F and Cellulose Acetate 3.0 µm).*

The flow pattern of bovine Hb on ten different paper materials are shown in *Figure 4*. The desired performance is to have a consistent and clean flow track on the paper. As a starting point for developing a rapid test, the desired time for bovine Hb to flow across the distance of 6 cm is within 20 minutes. Observed by eye, the migration of bovine Hb with the fluid flow toward the absorbent pad was minimal within 20 minutes on filter paper 3, filter paper 5, and CF2. On GF/F, bovine Hb disperses to the sides of the paper more compared to others, leading to a wider flow track. The width of the flow tracks of bovine Hb on the remaining papers were about the same by eye. Cellulose acetate, which is used in the HemeChip for 1D electrophoresis, was also tested [33]. However, it became wrinkled after the running buffer passed through, which is not ideal for constructing complex paper geometry. Comparing Grade 691, Grade 693, MF1, and FUSION5, bovine Hb flowed most consistently on Grade 691. As bovine Hb flowed through Grade 691, the change in dot shape and the tailing were the least. The material with the most consistent and cleanest flow pattern was chosen as the testing paper for further experiments. Therefore, Grade 691 was chosen as the testing paper for further experiments.

However, in later experiments, it was found that the pH of the running buffer affects the affinity of Grade 691 for proteins. Therefore, it may not be an ideal material choice. This will be discussed further in Chapter 3.6.

Diffusion vs Paper Material (Dispersion & Volume-Holding Capacity)

The horizontal spreading on the paper may result from both diffusion and dispersion. An estimation of the diffusion component was made using the mean squared displacement equation from random walk theory [52].

$$x^2 = 2dDt$$

where x is the displacement of the particles, d is the dimensionality, D is the diffusion coefficient, and t is the time. The diffusion coefficient was estimated using a reported value of $67x10^{-8}$ cm^2/sec, which corresponds to a hemoglobin concentration of 20 g/L at 20-22 degrees C [53]. The flow test was conducted using 15g/L of hemoglobin concentration, which is close to the 20 g/L used in the diffusion coefficient reference.

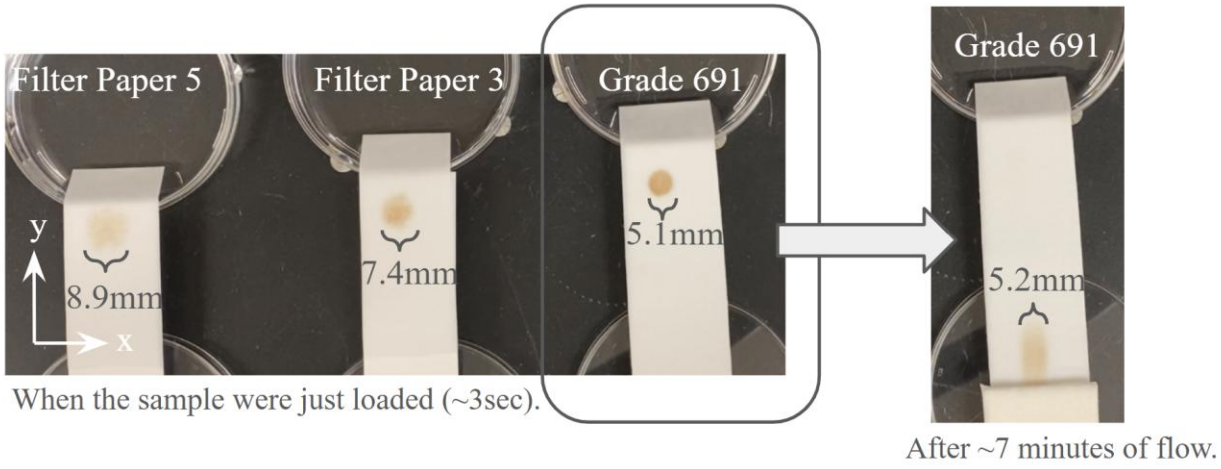

Figure5*: 0.1x Bovine Hb (15g/L) flow pattern on different paper materials (a zoomed in and annotated view of Figure4).*

Assuming a simplified 1D model, the estimated spread of bovine Hb in the x-axis direction caused by diffusion over 3 seconds is approximately 0.02 mm. (The x-axis is defined as the direction perpendicular to the flow, while y-axis is defined as the direction of the flow). In contrast, the initial spreading observed in *Figure 5*, across different materials when first dropped onto the paper, occurs on the scale of ~1 mm. This suggests that dispersion and volume holding capacity due to paper material plays a much bigger role in horizontal spreading. Additionally, for Grade 691, the spread in x-axis after 7 minutes of flow through the paper was measured. The estimated diffusion contribution over this time is approximately 0.24 mm. Experimentally, the spot width increased by about 0.1 mm, which is in the same order of magnitude as the calculated value. However, due to the presence of vertical flow, the actual horizontal spread may have been slightly

reduced. Although this is only a rough estimation, it indicates that material properties dominate the initial spreading behavior in this system, while diffusion may become more relevant over longer timescales. Therefore, selecting paper with minimal dispersion and larger volume-holding capacity in smaller area is critical to minimize the initial spreading.

Method: Paper Materials

Whatman filter paper 3 (6 μm pore size; CAT No. 1003-090), Whatman filter paper 5 (2.5 μm pore size; CAT No. 1005-090), Whatman FUSION5 (CAT No. 8151-9915), Whatman CF2 (CAT No. 8112-2250), ADVANTEC cellulose acetate (0.8 μm pore size and 3.0μm pore size; C080A090C and C300A090C), VWR Glass Microfiber Filter 693 (Grade 693; North American CAT No. 28297-510), VWR Glass Microfiber Filter 691(Grade 691; North American CAT No. 28297-289), and Whatman GF/F Glass Microfiber Filters (CAT No. 1825-090) were the testing paper material options that we selected from. The absorbent pad used was SureWick C083 Cellulose Fiber Sample Pad Sheets. The sample pad and buffer pad were scissors-cut 2 cm by 2 cm square Millipore Glass Fiber Diagnostic Pad (EMD; GFDX203000). Flow testing was performed on different papers to observe the flow movement of samples on each material. Each paper was scissors-cut into a 2 cm *7.5 cm rectangle. The end of the testing paper was 0.5 cm overlapped with the absorbent pad (scissor-cut into 2 cm *6 cm). The two components of the paper setup were held on a backing card (DCN Backing Card - 0.010” thick; scissor-cut into 2*8 cm). The head of the testing paper was submerged in the free fluid running buffer, 1x TBE (pH 8.3), that was contained in a petri dish. 1:10 diluted bovine Hb was loaded by pipetting 2 μL on each testing paper. Five testing papers were tested at the same time, with a 10 second interval between loading samples on each paper from left to right. The flow pattern was recorded by a phone camera. The dimensions were measured with ImageJ.

3.3 Continuously Loading Samples

Sample Wick

A sample wick was considered as the strategy to continuously load samples onto the testing paper. The sample wick is designed to be a thin triangle that acts as a bridge between the sample source and testing paper. Two desired properties were taken into account when deciding on the material and the shape of the wick. The first property is the direction of flow. The wick should be able to transfer the sample in the direction toward the testing paper, ultimately loading the sample onto it. The second property is the speed of loading samples. Slower sample loading is preferred since it results in thinner sample track on the testing paper. Both properties are controlled by the difference in capillary pressure between sample source, sample wick, and testing paper. The flow in the sample source to testing paper direction should be large enough to compete out the flow of the buffer from testing paper to the wick. Therefore, the larger flow rate is preferred in controlling the direction of flow. However, in terms of loading samples, faster flow rate will lead to broader sample track on testing paper. Therefore, a balance between the two properties were to be found when choosing the material and shape.

The sample wick could be modeled as fluid flowing through a porous medium by Darcy's Law:

$$q = -\frac{k}{\mu}\frac{\Delta P}{L}$$

where q is the flux, k is the permeability of the porous medium, ΔP is the pressure difference between the two ends, μ is the fluid viscosity, and L is the length of the flow path [54].

The volumetric flow rate is the flux time the cross-sectional area (A):

$$Q = qA = -A\frac{k}{\mu}\frac{\Delta P}{L}$$

And the permeability (k) is related to the pore size by the equation [55]:

$$k = c\varphi r^2$$

where c is geometric factor of the material, φ is the porosity, and r is the pore radius.

Here, we are not trying to determine the actual values of these parameters but instead are using their relationships to guide the design of the paper setup. From these equations, we know that the flow rate is proportional to the permeability of the material. It is also proportional to the cross-sectional area, which is affected by the thickness and width of the paper, and it is inversely proportional to the length of the material. The system is simplified by assuming the capillary pressures at both ends remains the same since the one end of the sample wick is connected to free fluid (sample source), and the other end is connected to the testing paper with the running buffer. The pore size of the material is modeled in the equation of permeability, with larger pore size having larger permeability. The length of the sample wick is modeled as the length L. Therefore, two strategies of controlling the flow rate were developed and tested. The first strategy is to vary the pore size by trying various paper materials as the wick. The second strategy is to control the wick length (triangle height) and use the same paper material as the testing paper. Bromophenol blue (BPB) was chosen to learn the sample loading performance since it is blue dye that can be easily visualized.

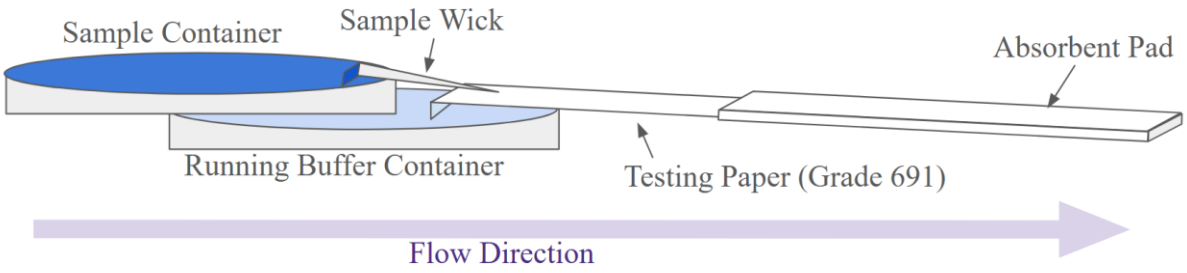

Figure 6*: Schematic of the setup for the flow test with sample wick.*

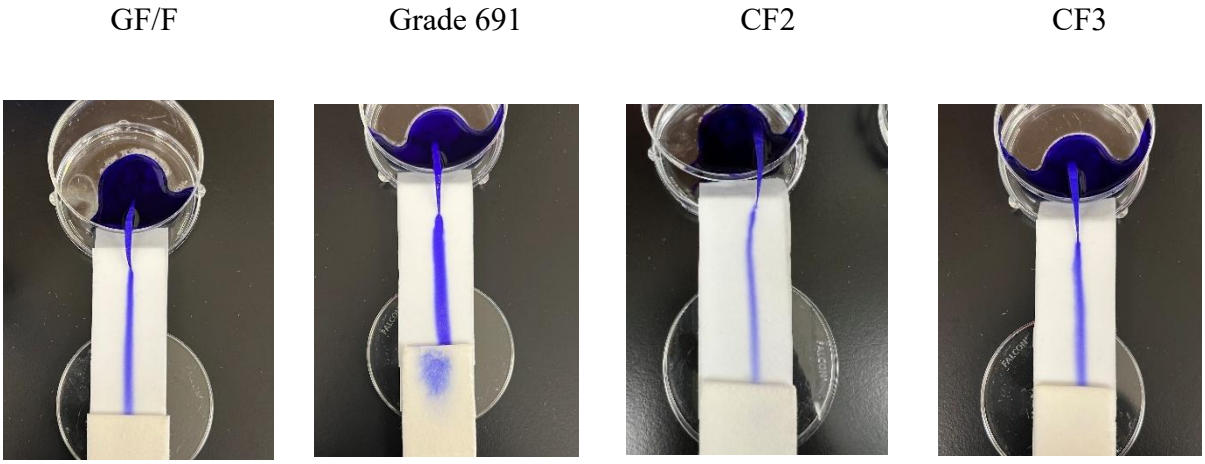

Figure 7: *Different sample wick materials continuously loading BPB on the Grade 691 testing paper.*

For the first strategy, among the wick materials tested, CF2 wick gave the thinnest track on Grade 691 testing paper as shown in *Figure 7*. However, given the complexity associated with incorporating additional material types into the system, adjusting the length and width of the paper material was regarded more feasible than changing the material itself. Thus, Grade 691 wick with a length of 4.5 cm was implemented, and the outcome of sample loading using this wick was satisfactory for subsequent experiments.

Sample Pad and Buffer Pad

Additionally, drawing fluid from another paper material rather than from free liquid source results in different loading rates. A sample pad was added to help hold the wick in place by sandwiching it between two loose glass fiber layers. Millipore Glass Fiber Diagnostic Pad material was chosen so that the fluid starts in a region with larger pore size and can flow into the testing paper, which has smaller pores. The addition of this pad increases the resistance for fluid to being drawn through the wick and loaded onto the testing paper. When only the sample pad was used and the running buffer was still drawn from free fluid, the testing paper tended to pull fluid primarily from the buffer side, since it was much easier (lower resistance) to draw fluid from the free liquid than from the sample pad. As a result, no sample was loaded onto the testing paper (*Figure 8, left*). When both a sample pad and a buffer pad were used, the sample was successfully loaded onto the testing paper (*Figure 8, right*). These results suggest that balancing the fluidic resistance between the sample source and buffer source is important for proper loading. These pads are also useful in the final device design to hold fluids in place and reduce leakage.

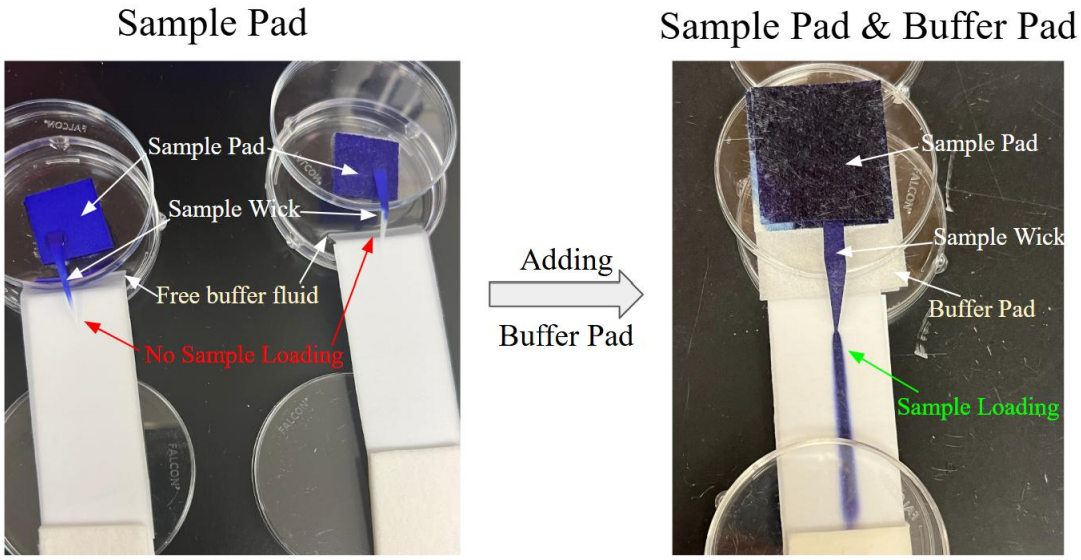

Figure 8*: Images captured from experiments testing the use of sample and buffer pads.*

Method: Continuously Load Sample and Sample/Buffer Pad

First, Whatman CF2, Whatman CF3, VWR Glass Microfiber Filter 691 (Grade 691), and Whatman GF/F were scissor-cut into a 0.2 cm *2 cm thin triangle shape. The testing paper Grade 691 was set up in the same way as in the Testing Paper Material Selection section. The sample source used here was free fluid of BPB, contained in another petri dish. The 0.2 cm side of the sample wick was submerged into the sample source and the vertex was contacted with the testing paper. Second, Grade 691 was scissor-cut into a thin triangle with the base of 0.3 cm and varied in height, which is the length of the wick. The sample wick was set up in the same way. The flow pattern was recorded by a phone camera. For the sample pad and buffer pad, Millipore Glass Fiber Diagnostic Pad (EMD; GFDX203000) was cut into pieces of square. Two pieces of them were used to sandwich either sample wick or the buffer inlet of the testing paper.

3.4 Buffer Inlet Paper Geometry for Discontinuous Buffer System

To explore the implementation of buffers with varying pH levels at the inlet to establish a pH gradient for the discontinuous buffer system, an experimental study utilizing red and blue dyes was conducted to observe and simulate the flow dynamics. As shown in *Figures 9-a* and *9-b*, blue and red dyes exhibited limited mixing at the interface, resulting in a narrow overlap of colors. On the other hand, *Figure 9-c*, employing an alternative inlet configuration by sandwiching the testing paper, demonstrated a broader and more extensive mixing of colors. This observation offers a strategic insight into different approaches for manipulating the buffer system in subsequent experiments.

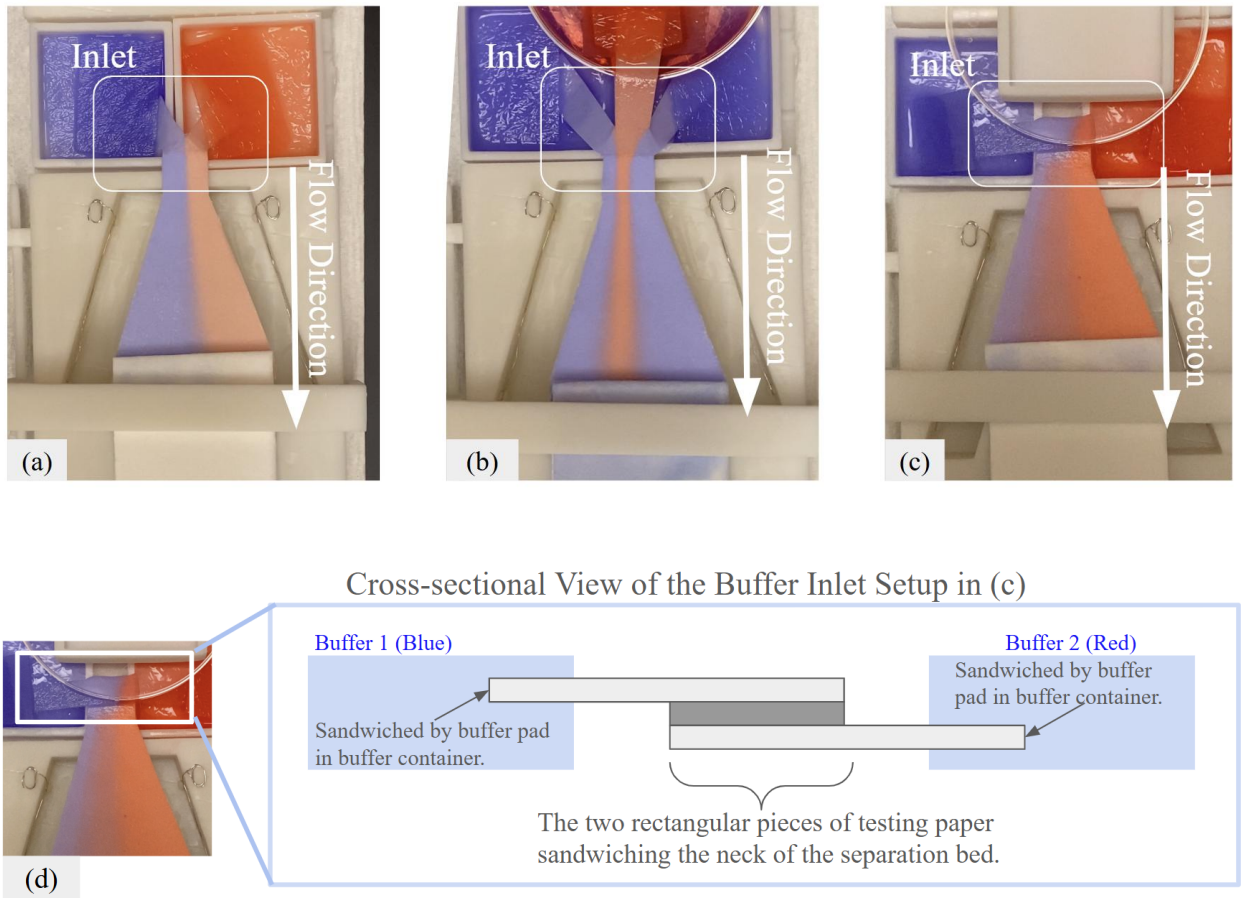

Figure 9: *Different methods of creating a pH gradient by adjusting buffer inlets. (Red: red food dye (RFD); Blue: BPB).*

Method: Buffer Inlet Paper Geometry

Grade 691 was scissors-cut into the geometries shown in *Figure 9*. The constant area of the testing paper begins with a 1 cm-long and 1 cm-wide neck, followed by a trapezoidal section with a 1 cm upper base, a 3.5 cm lower base, and a height of 4 cm. The lower 0.5 cm of this trapezoid overlaps with an absorbent pad with the dimension of 3.5 cm*6 cm. The variable area was the inlet. In Figure 9-a, the inlet consisted of two symmetrical branches fanning outward from the center of the neck, forming a V-shape. In *Figure 9-b*, there were three branches. The ends of the branches were immersed in the buffer container and sandwiched between two pieces of the Millipore Glass

Fiber Diagnostic Pad. In *Figure 9-c* and *9-d*, the inlet was composed of two separate pieces of Grade 691, each measuring 0.5 cm*2 cm. One end of each rectangular piece was immersed in the buffer container and sandwiched by Millipore Glass Fiber Diagnostic Pad, while the other end overlapped either on top of or below the neck, forming another sandwich structure with the neck in the middle. To ensure consistent contact between the three pieces of paper, a transparent Petri dish was placed on top for compression. These paper geometries were assembled on the backing card. Red food dye (RFD) and BPB were applied to the buffer container to start the flow. The flow pattern was recorded by a phone camera.

3.5 Platform Prototype

Combining the results above, an integrated paper setup was developed with components including sample pad, sample wick, buffer pad, separation bed, electrodes, and absorbent pad (*Figure 10*). The flow direction is controlled by establishing a gradient from large pore size material to small pore size material, utilizing differences in capillary pressure to drive the flow.

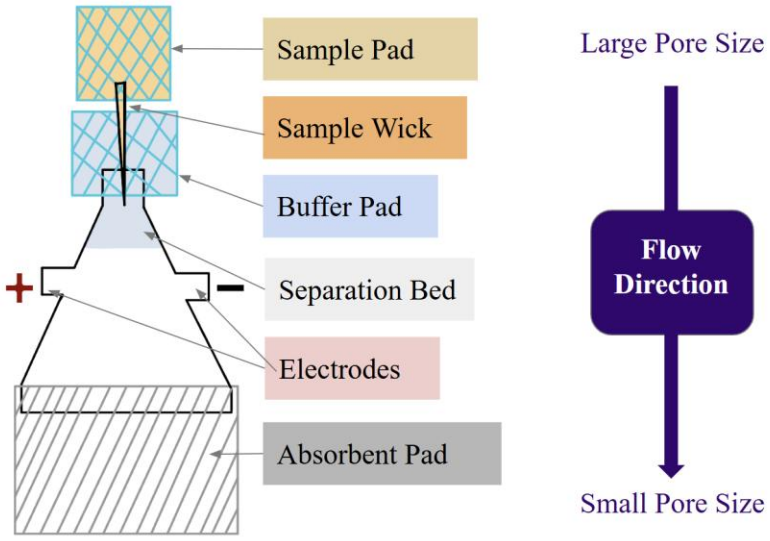

Figure 10: *Schematic of the integrated paper setup.*

The sample pad and buffer pad are separate inlets connected to the testing paper. The buffer pad is the source of running buffer and is in direct contact with the separation bed by the buffer inlet section, circled in *Figure 11-d*. The sample pad is connected to the testing paper with a sample wick to control the speed of loading the sample. The sample pad and buffer pad are composed of two layers of loose glass fiber that sandwich the separation bed buffer inlet or the sample wick between the two layers. This meant to ensure contact between them.

Two main versions of paper setup were developed, mainly changing how the separation bed is connected to the electrodes. In the first setup (Setup 1), the electrodes are directly clipped on the testing paper at the wings on the sides (*Figure 11-a*). The wings were designed to avoid electrodes interfering with fluid flow. In the second setup (Setup 2), electrodes were clipped on the platinum wire that is submerged in the buffer (*Figure 12-c).* At both sides of the Setup 2 testing paper, there is a curtain connecting the testing paper and electrodes by submerging one side into the buffer tank with buffer (*Figure 11-b*). Setup 2 was connected to the electrodes by having a paper curtain that had one side submerged in a buffer tank with electrodes and one side contact with the side of testing paper. This avoids the direct contact of the paper and electrodes, reducing the heating issue. Both setups allow exerting an electrical field orthogonal to the flow direction.

Three main portions of the testing paper were varied during the design iteration, which are the location of electrodes, neck (N5, N10), buffer inlet (I, II, III), and the separation bed length (*Figure* 11). Buffer inlet (I, II, III) was designed to accommodate different buffer systems. The separation bed was designed to be a trapezoidal shape due to the improvement shown in DF-IEF. The last portion of the paper setup is the absorbent pad, which absorbs the fluid and allows the fluid to flow in the direction from sample source to absorbent pad.

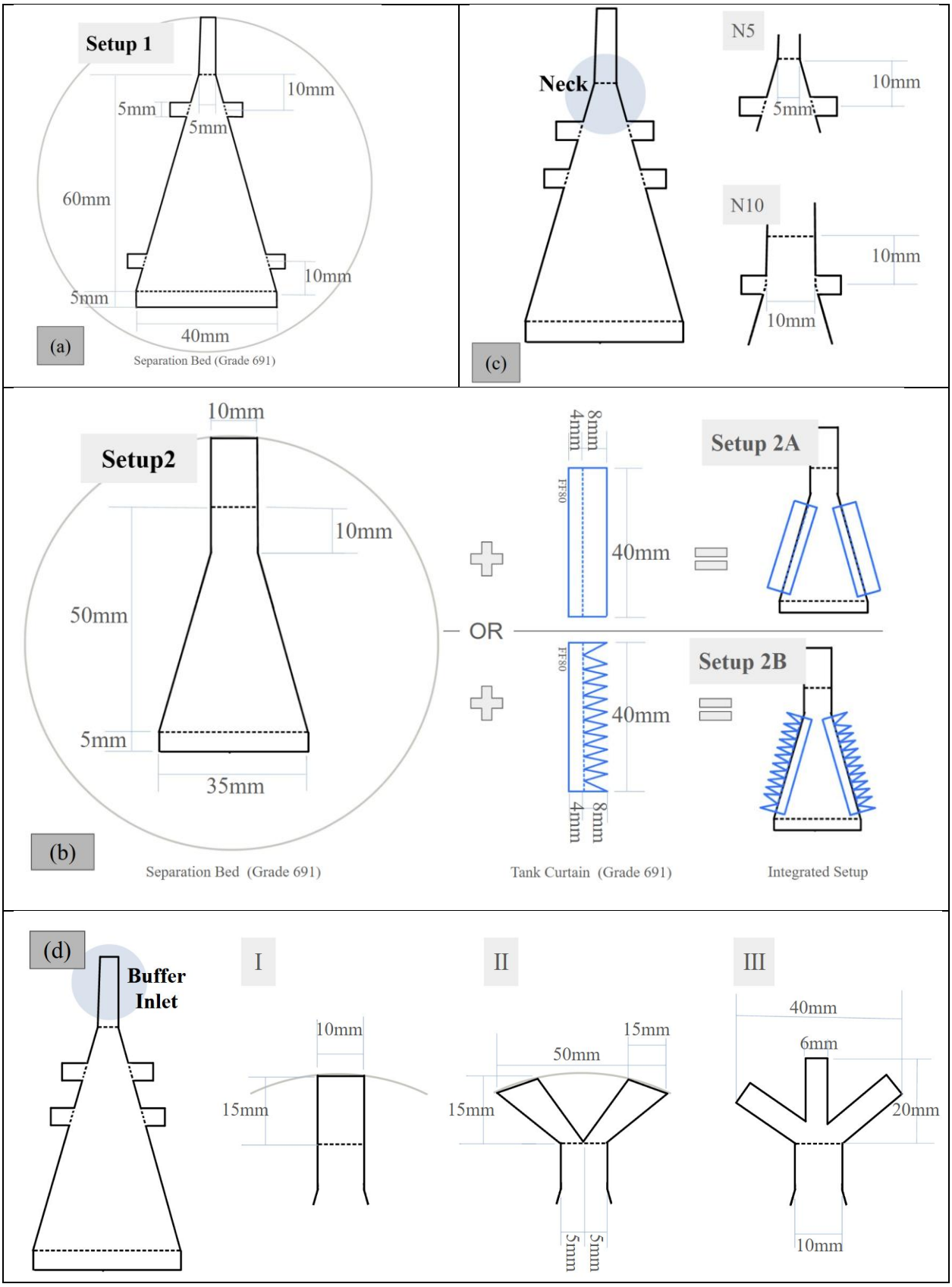
Setup 1
10mm
5mm
5mm
60mm
10mm
5mm
40mm
(a)
Separation Bed (Grade 691)
Neck
(c)
N5
10mm
5mm
N10
10mm
10mm
10mm
Setup2
10mm
50mm
5mm
35mm
(b)
Separation Bed (Grade 691)
OR
8mm
4mm
FT80
40mm
Setup 2A
FT80
40mm
8mm
4mm
Setup 2B
Tank Curtain (Grade 691)
Integrated Setup
(d)
Buffer Inlet
I
10mm
15mm
II
15mm
50mm
15mm
5mm
5mm
III
40mm
6mm
20mm
10mm

Figure 11: *Dimensions of multiple versions of the paper setup. (Not all dimensions are shown; further iterations exist, but all remain within a similar scale.)*

Two main iterations of cassette were developed for accommodating paper Setup 1 and Setup 2, respectively (*Figure 12- a*). The cassette was designed to hold the testing paper. The rotatable pressure bar was implemented to facilitate uniform contact between testing paper and absorbent pad and secure the paper setup in place. In Cassette 1, the trapezoidal platform was extruded from the surroundings to allocate space for electrode clips. This serves to mitigate any potential paper distortion caused by the clips, thus maintaining the flatness of the paper setup. In Cassette 2 (tank cassette), buffer tanks were situated on both sides of the trapezoidal platform. The curtain can hang down along the wall and remain partially submerged in the buffer in the tank. Platinum wires were coiled in the buffer tanks, extending outward from the tank to a small column onto which electrodes can be clipped on (*Figure 12 -c*). The cassette and buffer container were designed to accommodate setup for various buffer combinations. The rail on the cassette and the corresponding groove under the buffer container allow flexible placement of buffer containers. The square portion of the sample loading tray is designated to hold the sample pad, while the narrow triangular portion is reserved for holding sample wick. At the tip of the sample loading tray, the small guiding wall served to position the tips of the sample wick, thereby ensuring more consistent contact with the testing paper and uniform sample loading between trials.

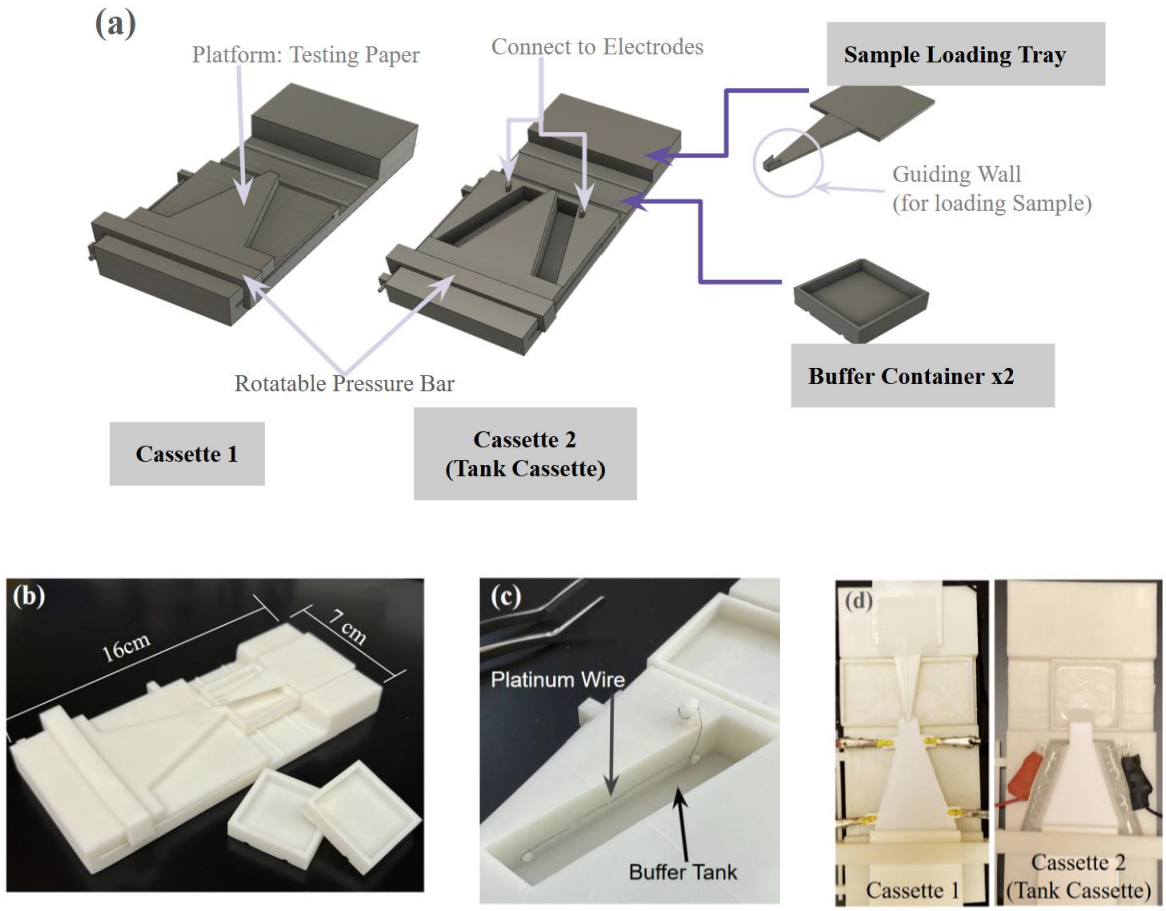

***Figure 12**: Schematics and pictures of the paper CFE platform cassette. (a) Schematic of 3D model cassettes (b) Photo of printed Cassette 1. (c) Photo of platinum wire coiled in the buffer tank in Cassette 2 (tank cassette). (d) Photo of the paper setup on the cassette with different ways of electrode connection.*

One important issue to be aware of is fluid channeling between the backing card and the cassette platform. This undesired flow creates a low-resistance pathway when voltage is applied, causing current to preferentially flow through that path rather than the separation bed. As a result, this can lead to a sudden increase in unstable current, which may pose safety risks and disturb the separation performance. There are two locations on the platform where channeling tends to occur, both of which were addressed by optimizing the integration between the cassette and paper setup.

First, at the buffer inlet where it is submerged into the buffer container, the buffer tends to wick underneath the backing card at the contact point. To prevent this, it is important to ensure that the backing card is not placed too close to the fluid surface. Additionally, positioning the buffer pad to hold the buffer in place helps prevent leakage under the backing card. The second location is in the tank cassette, where fluid can flow along the curtain and wick underneath the backing card through the gap between the curtain and the tank wall. To address this, designing the tank wall with a concave shape increases the distance between the curtain and the wall, helping to reduce unwanted flow along that gap.

Method: Paper Setup

Two types of integrated paper setup were designed for different ways to apply electrodes. Paper fabrication was performed by scissor-cutting or laser-cutting. The testing paper geometry at the running buffer inlet was varied to accommodate different buffer systems. The dimension of paper geometry was shown in *Figure* 11. *Note: the dimensions presented in the figure do not represent all versions used in this thesis. Various iterations with different dimensions were tested throughout the project, though the overall scale remains similar to what is shown here. For details on other paper geometries, please refer to Appendix 1.*

Setups 1 and 2 were combined with different geometry at neck and buffer inlet. For Setup 1, two pairs of electrodes were clipped on the wings on the side. Setup 2 was connected to the electrodes by having a paper curtain that had one side submerged in a buffer tank with electrodes and one side contact with the side of testing paper. The material used for the curtain was Whatman FF80HP Membranes (CAT No. 10547003). The absorption pads were cut into rectangles of 4 cm*6 cm and 3.5 cm*6 cm. Testing paper and absorption pad were contacted with 0.5 cm overlap. The upper half of the backing card was cut to the shape same as the testing paper but without the buffer

inlet portion, and the bottom portion was kept to support the contact between testing paper and the absorption pad. Testing paper and absorption pad were adhered onto the backing card. The electrodes were made with platinum wire obtained from a broken gel electrophoresis cassette.

Method: Cassette 3D model

The cassette to hold the paper setup was designed and 3D modeled by Autodesk® Fusion. The model was printed by stereolithography (SLA) 3D printing on Anycubic Photon Mono X. Eco UV Resin White was obtained from Shenzhen Anycubic Technology. The values within the recommended exposure setting from Anycubic were used, other values were set as default. After 3D printing, resin prints were washed with 100% isopropanol. The curing was done on Anycubic Wash&Cure Plus for 10 minutes.

3.6 Investigating Protein Retention on Grade 691: pH and Blocking Effects

In the later experiments described in Chapter 4, it was found that protein adhesion to Grade 691 occurred when the salt concentration was lowered. However, high salt concentrations are also not desired since it will disturb the pH gradient stability and compress the separation. (For details, please see Chapter 4.4). Also, it was observed that the adhesion of protein to paper seems to be different under different pH conditions. To troubleshoot this issue and better understand the underlying cause, a simple flow test was conducted using mCherry and HbA at different pH conditions (*Figure 13-a*). This allowed for observation of protein flow compared to dye flow under varying pH conditions in the absence of an electric field.

Flow Test of Proteins on Grade 691 at Different pH

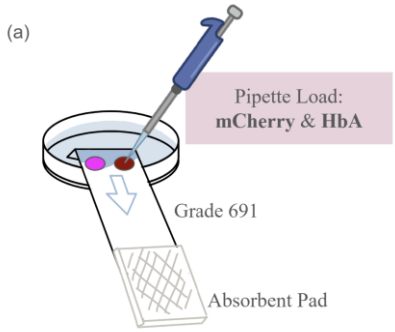

(b)	pH5.5 (Not Blocked)			pH6 (Not Blocked)			pH7.3 (Not Blocked)		
Time	0:00	5:00	10:00	0:00	5:00	10:00	0:00	5:00	10:00
mCherry (IEP =5.63)				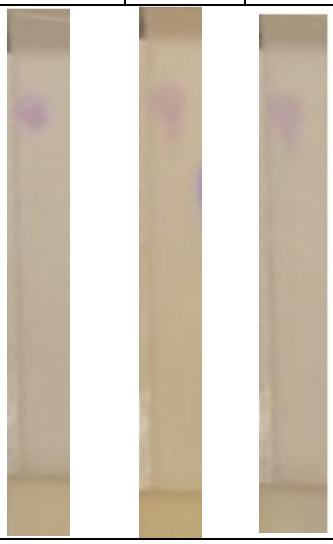					/
HbA (IEP =6.91)									

Figure 13*: (a)Schematic of the simple flow test method. "Created with BioRender.com". (b) Images of the simple flow test on mCherry and HbA with different pH at different time points.*

As seen in *Figure 13-b*, mCherry did not flow effectively under pH 5.5 and pH 6 conditions, but it migrated successfully without noticeable tailing at pH 7.3. For HbA, slight movement with tailing was observed at pH 5.5, no movement at pH 6, and clear migration with significant tailing at pH 7.3. These results suggest that at pH values close to each protein's IEP, the proteins become nearly neutrally charged and tend to precipitate, especially under no-salt conditions. In low- or no-salt environments, protein solubility increases as salt concentration increases due to charge screening; this is called salting-in. The salting-in region of hemoglobin is reported to be below approximately 0.15M salt [56]. Therefore, having a moderate salt concentration can improve protein solubility by reducing aggregation. Additionally, successful migration on Grade 691 may require a sufficiently large difference between the pH and the protein's IEP, as seen in the case of mCherry (pH 7.3 vs. IEP 5.63). However, HbA (IEP 6.91) did not migrate well at pH 5.5, even though the pH difference is comparable. This may be due to the nature of Grade 691, which is made of glass fiber and carries a negative surface charge under neutral and basic conditions [57]. At pH values lower than the IEP, proteins are positively charged and may adhere more strongly to the negatively charged paper, leading to retention and tailing. Under higher salt conditions, the presence of salt ions may help by coating the surface of Grade 691 or by screening electrostatic interactions, thus reducing nonspecific binding between the protein and the paper surface.

Assessing Whether Blocking Grade 691 Enhances Protein Flow

pH6	Not Blocked		1% BSA		1% BSA + 0.1%Tween20	
Time	0:00	5:00	0:00	5:00	0:00	5:00
mCherry (IEP=5.63)	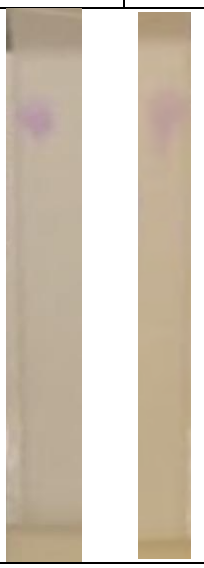				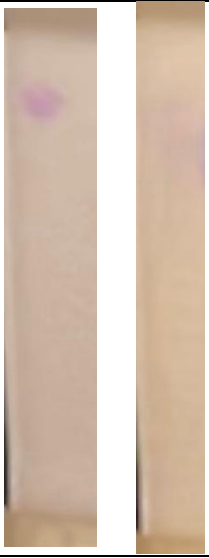	
HbA (IEP=6.91)	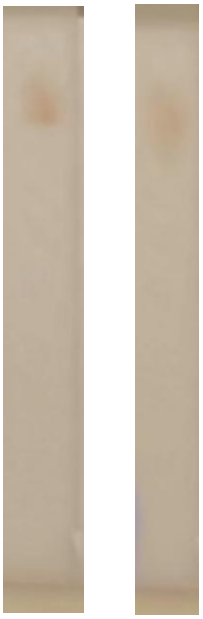		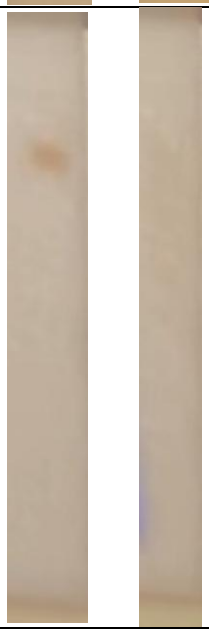		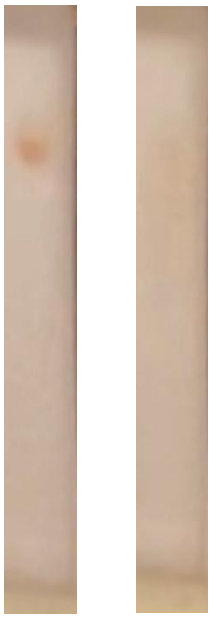	

Figure 14*: Images of the simple flow test on mCherry and HbA with pH6 with different surface treatment at different time points.*

Since adhesion and precipitation issues are hindering protein flow on Grade 691 at different pH levels, and because we want to control protein movement by setting specific pH values (see Chapter 4.2 for details), we aimed to address the problem of surface adhesion. Two surface

treatments were applied to Grade 691, and a simple flow test was conducted to evaluate whether they helped (*Figure 14*). The first condition involved blocking the surface of Grade 691 with 1% BSA. The second condition combined 1% BSA with 0.1% Tween 20 to reduce protein aggregation and precipitation. *Figure 14* shows the flow test results at pH 6, where both mCherry and HbA initially showed no movement. These results were compared to the flow tests under the two blocking treatments.

In both treated conditions, the proteins moved but left faint pink or red traces behind their paths, slightly visible in the images captured at 5 minutes. However, there was little difference between the condition with Tween 20 and the one without it observed by eye. These results suggest that blocking the surface improved protein flow on Grade 691, but the treatment may not be effective enough to fully eliminate tailing or adhesion.

Method

Blocking was performed by first preparing 1% BSA and 0.1% Tween 20 solutions. The paper was soaked in either 1% BSA or 1% BSA + 0.1% Tween 20 for 1 hour, then washed with water and dried overnight. The paper setup for the flow test was the same as previously described. The running buffer was 10 mM histidine buffer at different pH values. HbA and mCherry were loaded onto the paper using 1 μL volumes. The flow pattern was recorded using a phone camera. To improve visibility and interpretability, the image saturation and contrast settings was adjusted in *Figures 13* and *14*.

3.7 Conclusion

In this chapter, a functional paper-based platform for continuous flow electrophoresis was developed through systematic design and iteration. The platform utilized capillary-driven flow by creating a pore-size gradient across materials to control flow direction and rate without external

pumps. Material screening identified Grade 691 as the most promising paper for the separation bed due to its consistent, clean flow patterns, and wide heat tolerance under standard conditions. However, subsequent experiments revealed that protein migration on Grade 691 can be inhibited by protein adsorption under some pH conditions and salt concentrations. Near each protein's isoelectric point, especially under low-salt conditions, strong adhesion and precipitation were observed, preventing effective flow and leading to tailing. These issues are likely due to both reduced solubility near the IEP and electrostatic interactions between positively charged proteins and the negatively charged glass fiber surface of Grade 691. Surface blocking treatments using 1% BSA with or without 0.1% Tween 20 partially improved protein mobility but did not completely eliminate tailing or surface interaction. These results suggest that while Grade 691 performed well in early flow tests, it may not be an ideal material for applications requiring different pH setup and minimal protein–surface interaction. In future work, alternative paper materials with protein–surface may be explored to improve separation performance (see Chapter 5 for further discussion).

CH4 Analytes Separation on Miniaturized Paper CFE

4.1 Overview of Buffer Systems

In order to achieve separation of analytes under a small scale and small voltage, the composition of the running buffer became a variable for manipulation. Three distinct buffer systems were employed on the platform to assess their feasibility and gather insights for further design refinements. The buffer systems applied include single buffer system, discontinuous buffer system, and free-flow field step electrophoresis (FFFSE) (*Figure 15*). Additionally, a combination of the discontinuous buffer system and FFFSE was also investigated.

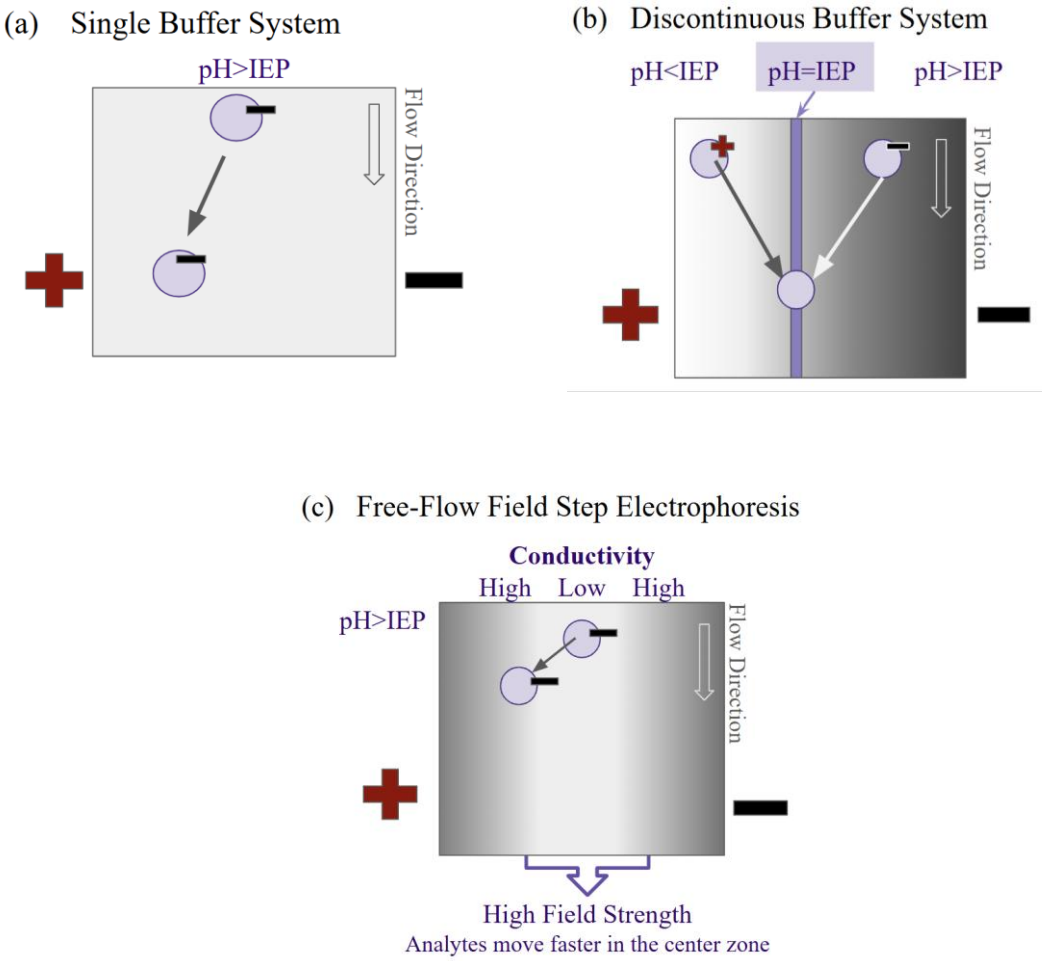

Figure 15: (a) *Single buffer system.* ***(b)*** *Discontinuous buffer system.* ***(c)*** *Free-Flow Field Step Electrophoresis (FFFSE).*

IEP is the pH at which the net charge of a particle is zero. The magnitude and polarity of particle net charge under the influence of an electric field is determined by its difference between the medium pH and its own IEP. The particle will carry positive charge when pH <IEP, neutral charge when pH=IEP, and negative charge when pH>IEP. For particles with multiple ionizable groups, a greater difference between pH and IEP leads to a greater net charge due to increased protonation or deprotonation. Electrophoretic mobility (μ) of a particle under the field is

$$\mu = \frac{\vec{v}}{\vec{E}} = \frac{q}{f}$$

where **v** is the electrophoretic velocity, **E** is the electric field strength, q is the net charge under **E**, and f is Stokes Frictional Factor modeling the particle as a sphere [39]. These are the key factors that affect how the particle moves in the system, and the three buffer systems can separate analytes based on slightly different principles based on these factors.

Single Buffer System

The single buffer is the system that is used in zone electrophoresis. In a single buffer system, the direction of particle deflection towards the electrodes depends on the charge it carries relative to the surrounding buffer pH. Particles with stronger net charges experience stronger electric forces. The electric force exerted on particles with larger net charge will be stronger. Assuming similar analyte masses, according to Newton's second law, particles with larger net charges will move faster towards the electrode. The difference in this electrophoretic velocity is the main principle of

separating analytes in a single buffer system. This type of separation principle is used in the traditional diagnostic method of cellulose acetate electrophoresis at alkaline pH.

Discontinuous Buffer System

In discontinuous buffer system, pH gradient is built by having multiple buffer inlets at different pH. Separation occurs through isoelectric focusing, as an electric field is applied across a medium containing a pH gradient. Particles within this medium migrate towards electrodes of opposite charge until their net charge reaches zero and are focused at the location where pH=IEP.

Free-Flow Field Step Electrophoresis (FFFSE)

FFFSE is a strategy to increase separation at the center zone in CFE. According to conservation of current density,

$$\nabla \boldsymbol{i} = \nabla(\sigma \boldsymbol{E}) = 0$$

stronger field strength at the center is established by implementing a less conductive medium at the center zone, while employing more conductive media at sides [39]. This approach could facilitate separation without increasing the applied voltage.

Buffering Agent

To support these buffer systems and enable controlled analyte separation, buffering agents were selected based on their buffering pH ranges, ionic strength, and compatibility with proteins under electrophoresis conditions. Three buffering agents were used in this project: TBE (Tris-Borate-EDTA), ACES (N-(2-Acetamido)-2-aminoethanesulfonic acid), and Histidine Buffer.

TBE buffer is a running buffer that is commonly used in zone electrophoresis. The buffering range of Tris is pH 7 to 9, and that of boric acid is pH 8 to 10 [58]. TBE buffer is often

used at pH 8.3. However, TBE is more commonly used for nucleic acids, and its buffering range does not cover the desired range for later designs. Therefore, other buffering agents were explored. ACES buffer is a zwitterionic buffer with a buffering range of pH 6.1 to 7.5, which includes the desirable range both above and below the isoelectric points of hemoglobin variants, making it suitable for the buffer setup discussed in Chapter 4.2 [59]. Since it is zwitterionic, it does not carry current, which is helpful in IEF to improve separation. It is also considered a buffer with high electrophoretic reserve capacity (ERC), which is defined as the ratio of neutral species to total buffer concentration [60]. A higher ERC allows the buffer to better maintain its position and support a stable pH distribution. Histidine buffer is both zwitterionic and ampholytic, meaning that it can possess positive charge or negative charge, with a buffering range of pH 5.5 to 7.4, which also includes the desired pH range for further setups [61]. It is zwitterionic at its IEP, where the net charge is neutral, but the molecule carries both a positive and a negative charge. Due to its ampholytic nature, histidine can change its charge depending on the surrounding pH relative to its IEP. As an ampholyte, it can self-focus and help form pH gradients when used as a carrier ampholyte in IEF. The choice of buffering agent is important when aiming to build a desirable and stable pH gradient, which will be further discussed in Chapter 4.3.

4.2 Results and Discussion of Buffer System Performance

To evaluate which buffer system is most suitable, experiments were conducted using the three buffer systems introduced in Chapter 4.1: the single buffer system, discontinuous buffer systems, and FFFSE.

Single Buffer System

First, the objective was to identify the buffer pH at which HbA would exhibit noticeable deflection toward either electrode. A voltage of 30 V was uniformly applied across 1 cm of testing

paper by one pair of electrodes. In *Figure 16*, sample locations at various time points were analyzed based on gray values, where lower gray values correspond to higher color intensity on the testing paper. Therefore, the downward-concave peaks in the middle of the plots indicate the sample locations. The expected behavior of HbA was anticipated to deflect toward the positive electrode when the pH was below its estimated IEP, and toward the negative electrode when the pH exceeded its estimated IEP. However, observing by eye, HbA migrated straight down along the flow direction across all four pH conditions tested. According to the four plots in *Figure 16*, the majority of peaks overlapped, and no trend of migrating toward negative electrodes as the pH increase was observed. Electrophoretic mobility is based on the net charge carried on HbA. The net charge is based on the disparity between sample IEP and environment pH. Greater disparities result in larger net charges. Nevertheless, even by increasing the disparity between IEP and pH through testing at pH 8.0, no deflection toward the negative electrode was perceptible by eye or in the plotted data under 30 V with one pair of electrodes across 1 cm wide distance.

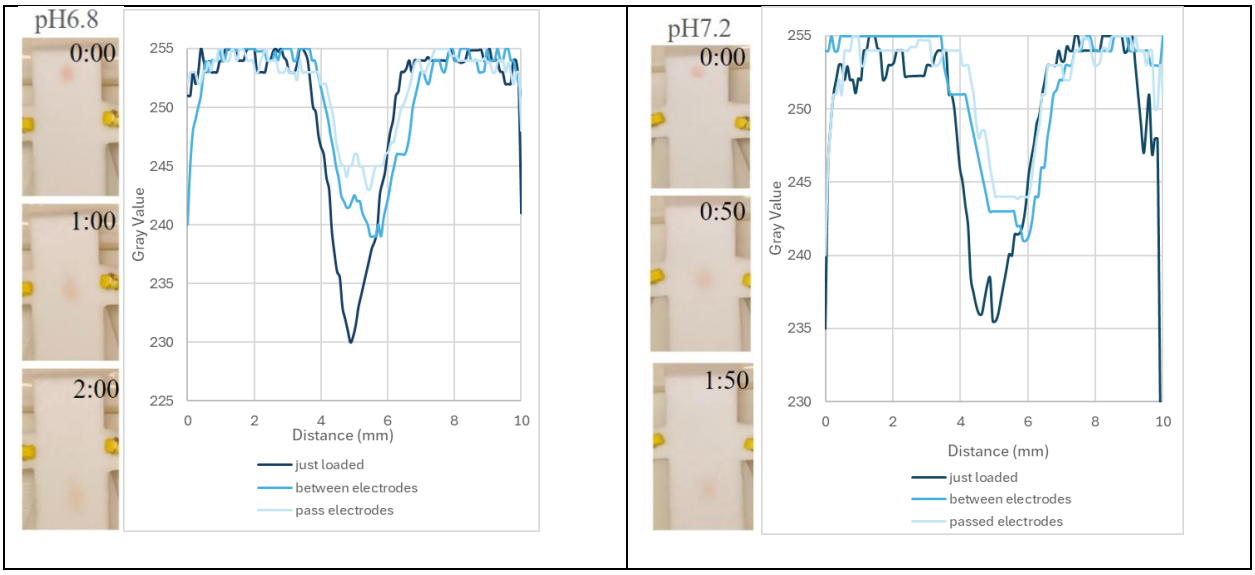

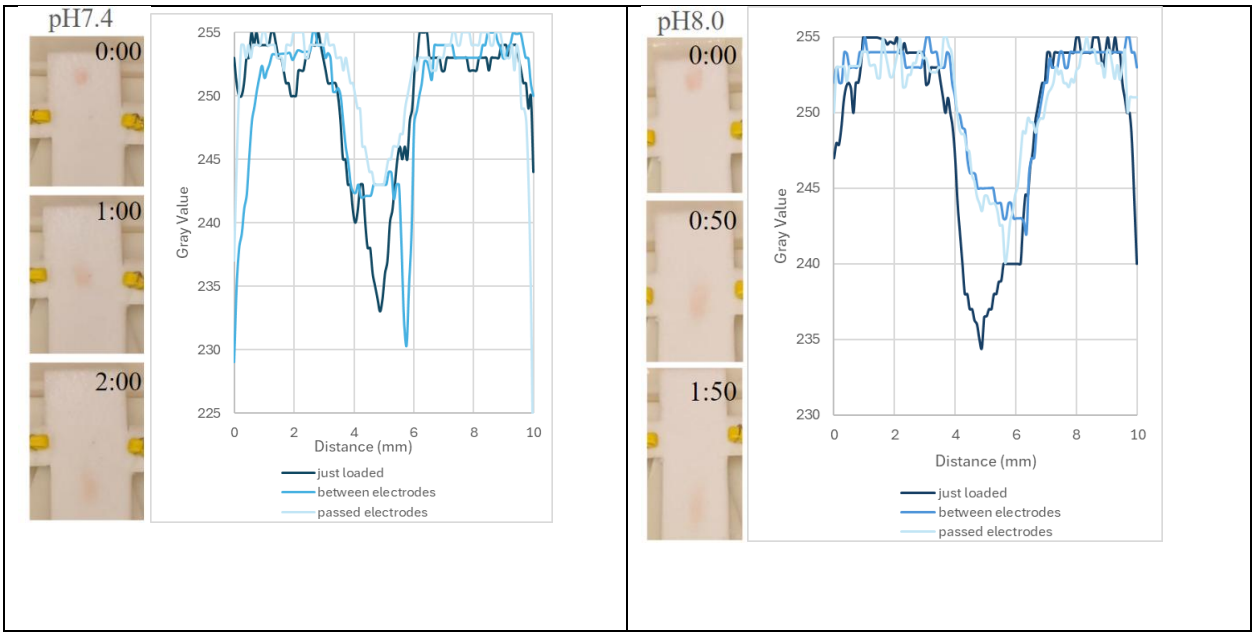

***Figure 16**: Sample locations at different time points. The concave downward peaks represent the horizontal distance of the sample to the side of the testing paper. The captured time points were right after the sample was loaded, when the sample was in between the electrodes, and after the sample passed the electrodes. The time points were noted on the images as minutes:seconds, and were noted on the plot from dark to light color. (Condition: 5x TBE (pH 6.8, 7.2, 7.4, 8.0); pipette loading 1 µL HbA (1:100); 30 V, right (+), left(-)).*

Therefore, a higher voltage, longer electrode contact, and a trapezoidal separation bed were employed to increase electric field strength and enhance separation. Setup 2, along with the tank cassette, was used to achive this while preventing paper buring at high voltage. This setup allowed the electric field to be aplied across the entire path of sample migration, thereby extending the duration during which the sample was subjected to the field. The voltage of 50 V was applied to the system. The duration from loading of the first sample to the last sample reaching the absorbent pad was approximately 13 minutes. Human HbA and HbS were introduced onto the platform under different buffer pH conditions as shown in *Figure 17*.

When the running buffer was at pH 6.5, both HbA and HbS (with isoelectric points above 6.5) carried positive charges and deflected toward the negative electrode, as expected (*Figure 17-a*). At pH 7.0, which lies between the IEPs of HbA and HbS, HbA was expected to carry a negative charge and HbS a positive charge. However, no clear deflection toward either electrode was observed (*Figure 17-b*), indicating no separation between them. At pH 7.5, where both HbA and HbS have IEPs lower than the buffer pH, both proteins should carry negative charges and migrate toward the positive electrode. While both deflected in that direction (*Figure 17-c*), no separation was observed between them.

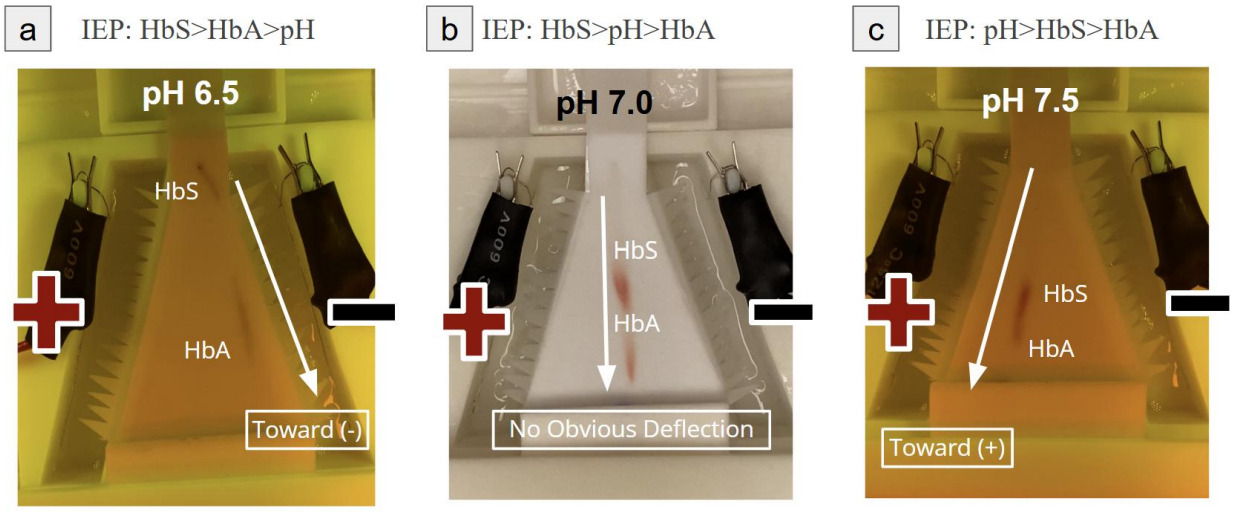

Figure 17*: Single buffer system applied on the tank cassette setup (Setup2). Sample (point loaded): HbA (1 µL), HbS (1 µL); Voltage: 50 V; Buffer: 100 mM ACES + 500 mM NaCl. The images were captured within the 12-minute video at the time point where three samples could be seen at the same time. The sample location was analyzed right before each sample reached the end of the testing paper (where the testing paper width = 35 mm).*

Discontinuous Buffer System

Next, discontinuous buffer system was evaluated. BPB, bovine Hb, and human HbA and HbS were applied on the platform. BPB is a low molecular weight dye that carries a negative charge under at neutral pH and becomes neutral under pH 4 [62]. It is also a pH indicator that appears blue at neutral pH and gradually shifts to yellow as the pH decreases from pH 4.6 to pH 3.0.

In a discontinuous buffer system, the samples separated primarily based on the principle of isoelectric focusing. *Figure 18-a* demonstrates a trend of BPB and bovine Hb separating under a single buffer system with the voltage of 50 V and two pairs of electrodes, wherein the blue color (BPB) was observed at the left and the brown color (bovine Hb) is on the right side. However, significant overlap occurred between them, indicated by the gradient of blue to brown color, resulting in only one peak in the grayscale intensity plot. When implementing a discontinuous buffer system with two buffer inlets, an improvement in separation is achieved (*Figure 18-b*). The sample became more focused on pH values corresponding to their IEP, where they are charge-neutral. This led to narrower track and more obvious separation of BPB and bovine Hb. The successful separation is indicated by the presence of two distinguishable peaks in the plot. In *Figure 18-c*, separation between BPB and Human Hb was observed. Despite this separation, separation between different Hb variants was not achieved under this condition. This observation implies that further optimization or alternative conditions may be required to achieve resolution between Hb variants.

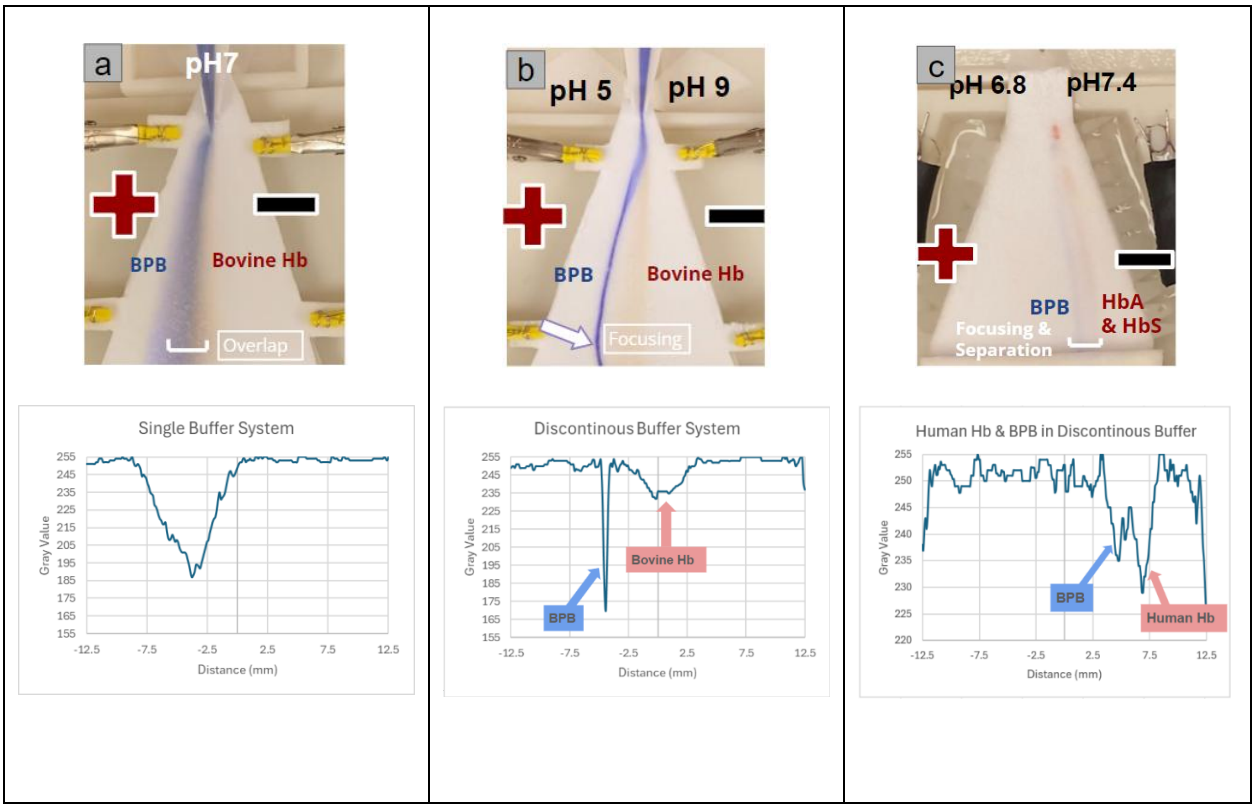

Figure 18*: Comparison between single buffer system and discontinuous buffer system.* ***(a)*** *Setup1A-N5-I* ***(b)****Setup1A-N5-II.* ***(a)(b)*** *Sample (continuously loaded): BPB, Bovine Hb (IEP=7.1)* [63]*; Voltage: 30 V; Buffer: 5x TBE ; Testing Paper: Grade 691.* ***(c)*** *Setup 2B-N10-II. Sample (pipette loaded): BPB (0.2 µL), HbA (1 µL), HbS (1 µL); Voltage: 50 V; Buffer: 100 mM ACES + 500 mM NaCl; Testing Paper: Grade 691.* ***(a)(b)(c)*** *The plots show the sample's spatial distribution at the horizontal cross-section located in the middle of the testing paper, where the width measures 25 mm.*

Free-Flow Field Step Electrophoresis (FFFSE)

FFFSE was implemented on the platform by introducing buffers with different conductivities through the three inlets to the separation bed, as shown in *Figure 11 d-III*. The conductivity differences were achieved by the varying the buffer concentrations. With only FFFSE

applied at pH 8.4, BPB and RFD deflected toward positive electrodes *(Figure 19-a)*. Bovine Hb and HbA exhibited migration along the center track. As the sample migrated down the testing paper, the sample track became wider. An attempt was made to combine FFFSE with discontinuous buffer systems and learn its viability *(Figure 19-b)*. The samples indicated that they were affected by the field, as shown by the focusing of the sample, resulting in a thinner track.

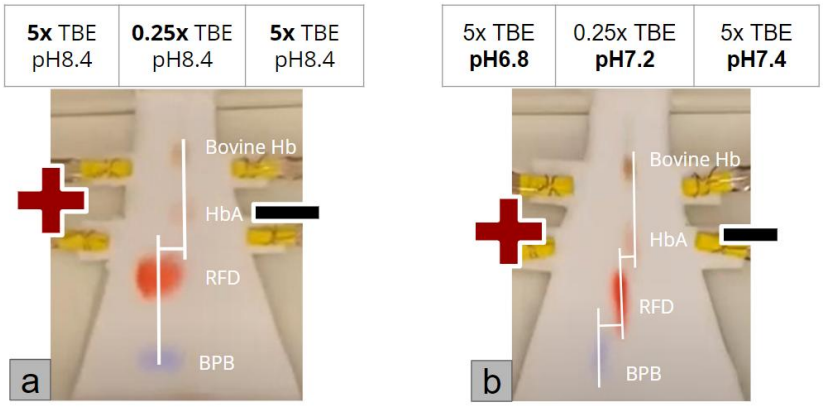

Figure 19*: FFFSE on Setup 1B-N10-III. Sample (pipette loaded): BPB 0.2 µL, RFD 0.2 µL, HbA 1 µL, Bovine Hb 1 µL; Voltage: 30 V; Buffer: 5x TBE and 0.25x TBE; Testing Paper: Whatman Grade 691.* ***(a)*** *FFFSE.* ***(b)*** *FFFSE combined with the discontinuous buffer system.*

Discussion of the Three Buffer Systems

Based on the results from the single buffer system, we observed that applying 30 V across a 1 cm separation bed with only one pair of electrodes was not sufficient to cause obvious deflection of HbA during its migration. In contrast, when 50 V was applied with a longer contact between the paper and the electrodes, clear deflection of Hb under different pH conditions was observed. This indicates that prolonged electrode contact is a desirable design feature, as it increases the duration of field exposure for analytes. The electrophoretic mobility of Hb is sufficient to show deflection in this platform. The observed deflection toward different electrodes

also confirms that we can control migration direction by adjusting the buffer pH relative to the IEP of the protein. However, the difference in electrophoretic mobility between HbA and HbS is not sufficient for separation under single buffer system.

In the discontinuous buffer system section, there is a direct comparison of single buffer system and discontinuous buffer system under same voltage (30 V) and same buffering agent (5x TBE). The results showed improved spatial separation of BPB and bovine Hb. The analytes were more sharply focused, with BPB and bovine Hb appearing as two clearly distinguishable peaks in the intensity profile. Further focusing of hemoglobin was observed when 50 V and extended electrode contact were applied *(Figure 18)*. Both the discontinuous buffer system and FFFSE demonstrated successful separation of the low molecular weight dye from the proteins. This marks an important first step in demonstrating separation capabilities. The next goal of this project is to separate two proteins, which have higher molecular weights. Based on the results so far, we propose that achieving this will require more precise pH control using a discontinuous buffer system and extended or increased contact with electrodes.

Proposed Buffer System for Protein Separation

The proposed concept is illustrated in *Figure 20*. Assuming two proteins with different IEPs (IEP1 < IEP2), we design the buffer zones in three sections. The left zone, near the positive electrode, is set to a pH below IEP1. The middle zone has a pH between IEP1 and IEP2, and the right zone has a pH above IEP2. Using the three-inlet geometry shown in *Figure 6b*, we can form two pH interfaces. Each protein will be focused at the interface sandwich by buffer zones with pH values just above and below its IEP, enabling spatial separation of the two proteins. FFFSE was not selected for this application because analytes in FFFSE tend to focus at the conductivity interfaces. If more than two proteins with different IEPs need to be separated in the future, the

number of conductivity interfaces may be insufficient to achieve effective separation. Additionally, study showed that isoelectric focusing (correspond to the discontinuous buffer system) have higher specificity and sensitivity in detecting SCD, compared to the zone electrophoresis (single buffer system) [64].

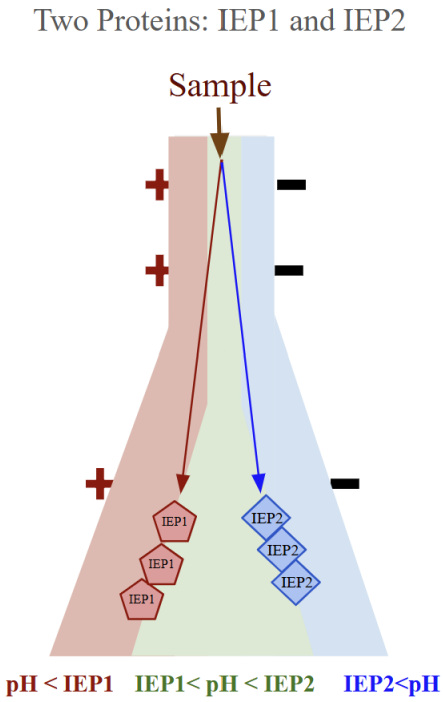

***Figure 20**: The proposed buffer system for protein separation.*

Observed Issue in pH Distribution Control

During experiments using the proposed buffer system, the desired separation was not achieved. The analytes did not migrate to the expected locations corresponding to the interfaces observed in the flow test (no voltage) with colored dyes. Additionally, as shown in the results for the discontinuous buffer system *(Figure 18),* although separation was observed, the entire migration region was shifted to the right when comparing *Figures 18-b* and *18-c*. This shift was

substantial and consistently observed across multiple experiments, suggesting it was unlikely to be caused by inconsistencies in the paper setup, such as uneven contact with the absorbent pad (a pressure bar was used in the cassette to ensure consistent contact between the absorbent pad and the separation bed). It was suspected that the expected pH steps were not properly formed. To investigate this, a quick test was conducted to assess the pH gradient on the separation bed after a run, using the pH indicator property of BPB. After electrophoresis and once the power was turned off, BPB was pipetted onto multiple locations along the separation bed. The inlet buffers were set to pH 6.5, 7.0, and 8.0. However, as shown in *Figure 21*, the BPB exhibited an abrupt color change in the middle of the strip, indicating a sudden shift from a region with pH below 3.0 to pH above 4.6. This result shows the need for a reliable method to monitor pH within the system in order to troubleshoot and establish stable pH steps or gradients. This method will be discussed further in Chapter 4.4.

Figure 21: *An image showing pH shift after a run with initial pH at the three buffer inlets were set to be pH 6.5, 7.0, 8.0 (running buffer: 100 mM ACES + 500 mM NaCl), indicated by the color change of BPB.*

Method: Testing Different Buffer Systems

Buffers were adjusted to different pH and various combinations of buffers were tested. First, 2 mL of running buffer was added to each buffer pad in the buffer container, allowing the running buffer to wet out the testing paper. For Cassette 2, 4 mL of buffer was added into each tank after the testing paper was wetted out. The samples were loaded on the testing paper either by sample wick or pipetting. Sample loading methods include pipetting a spot on testing paper, or continuously loading the sample on testing paper. For continuously loading the samples, 2 mL of mixed samples were added on the sample pad on the tray. BIO-RAD PowerPac Basic was used to generate potential differences across the testing paper. The flow pattern of the sample was recorded by a phone camera.

Analytes with visible color and different electrophoretic properties were applied on the paper platform. Bromophenol blue (reagent ACS; Cat. No: 032641.06) was obtained from Thermo Scientific Chemicals and prepared to 1 mg/mL concentration solution in water. Red food color (Ingredients: Water, Propylene Glycol, FD&C Reds 40 and 3, and 0.1 % Propylparaben (Preservative)) was obtained from McCormick. Hemoglobin from bovine blood (lyophilized powder; H2500), Hemoglobin A0 (Ferrous Stabilized human; H0267), and Hemoglobin S (Ferrous Stabilized human; H0392) was obtained from Sigma-Aldrich. Bovine hemoglobin (bovine Hb), Hemoglobin A0 (HbA), and Hemoglobin S (HbS) were prepared by resuspending in phosphate buffered saline (PBS pH 7.4 (1x); Gibco 10010-031) to 15 g/L (0.1x). The 15g/L stock Hb solutions were further diluted to 0.01x in water.

ImageJ was used to analyze the sample location on the testing paper as it migrated along the flow direction. An image was captured at a specific time point from the video. Subsequently, the image was converted into gray scale and subjected to background subtraction in ImageJ. Then

the scale was adjusted for dimension. The gray values were measured along a designated line and were plotted against the distance.

4.3 pH Gradient in Isoelectric Focusing

A stable pH gradient is essential for successful IEF, as analytes migrate and focus at the pH corresponding to their IEPs. Several strategies have been developed to establish pH gradients.

One common approach is the use of commercial carrier ampholytes, which are mixtures of small amphoteric molecules with overlapping pKa values [60]. When an electric field is applied, these molecules migrate and dynamically form a continuous pH gradient by releasing or accepting hydrogen ions along the way. This self-regulating process allows them to both adjust the local pH and migrate toward their own IEP, resulting in a steady-state distribution. While effective and widely used in IEF systems, carrier ampholytes are often expensive and less accessible in low-resource settings [65].

Another method involves immobilizing the pH gradient on a membrane using Immobilines [60]. These chemically defined buffering molecules are covalently bound to a polyacrylamide gel or membrane. Commercial immobilized pH gradient gels are available, but they are expensive and increase fabrication complexity.

A third strategy is to generate a pH gradient using acid-base titrants [60]. This is to build pH gradient based on binary pairs of known acids and bases. This method creates a stepwise pH gradient using binary pairs of known acids and bases. It is significantly more cost-effective than ampholyte-based systems. The principle relies on choosing buffer pairs with high electrophoretic reserve capacity (ERC), which is defined as the ratio of neutral species to the total buffer concentration. Buffers with high ERC (>0.9) consist primarily of neutral species, making them

slow-migrating molecules under an electric field. This property allows them to form more stable pH gradients. The pH range can be controlled by selecting buffer pairs with appropriate pKa values and high ERC. The Šlais group employed this strategy in their earlier work to construct a pH gradient [46].

Additionally, the Šlais group explored a different approach to generating a pH gradient without the use of carrier ampholytes in their DF-IEF system [48]. They demonstrated that complex biological samples, such as yeast lysate and flour extract, could form self-generated pH gradients through autofocusing. Since proteins are also ampholytes, the principle is similar to that of carrier ampholytes, as they can self-organize into a pH gradient under an electric field. However, this gradient is highly dependent on the composition of the sample, making it difficult to control. It is also nonlinear, with the neutral pH region often compressed. This behavior is not desirable for the design of my system.

In my system, rather than forming a continuous pH gradient, the proposed design creates a stepwise pH profile. In contrast to other methods that generate continuous pH gradients, this stepwise gradient is established through multiple buffer inlets. Therefore, the use of buffer pairs with high ERC is particularly suitable and can be effectively applied in this setup. The construction of a pH gradient using paper geometry provides a simpler approach that does not require expensive carrier ampholytes or a pre-focusing step, and allows for easier fabrication compared to immobilizing a pH gradient within the medium. The buffer inlet geometry design, as described in Chapter 3.4, also offers flexibility to create either a stepwise or continuous pH gradient.

4.4 Results and Discussion of pH Distribution Control

As mentioned in Chapter 4.2, there is a need to observe the pH distribution on this platform while it is operating. Using pH indicators may not be suitable, as they also move under the electric field and tend to focus. In addition, the available pH indicators only show a color change at a single transition point, making it difficult to capture the full pH profile across the separation bed.

pH Indicator Stamp Development

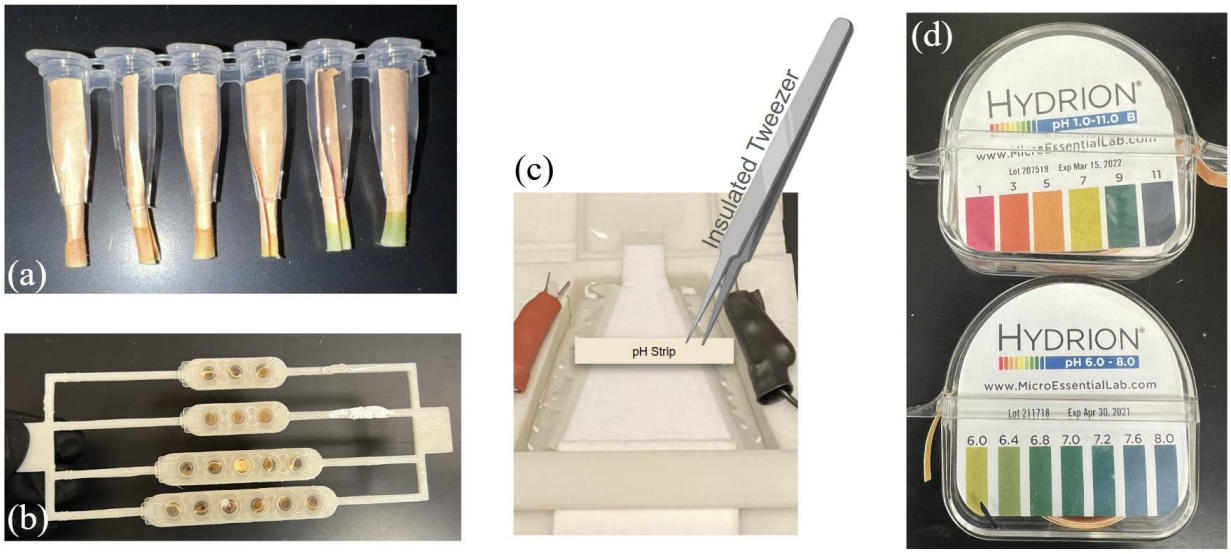

Figure 22*: Images of the pH indicator stamp. (a)(b) Using PCR tubes and a 3D-printed holder. (c) Using insulated tweezers and a small piece of pH indicator strip. "Created with BioRender.com" (d) The pH indicator strips used.*

To explore this, a stamp with pH strips was prepared (*Figure 22*). By stamping the pH indicator strips onto different locations at various time points during the run, we were able to assess the pH stability of the system. Two methods for stamping the pH indicator strips onto the separation bed were developed. The first method uses PCR tubes held in a 3D-printed holder, with pH indicator strips placed inside, and stamps them directly onto the separation bed (*Figure 22- a & b*).

The second method involves using insulated tweezers to press the pH indicator strip onto the bed, with one edge of the strip in contact with the surface (*Figure 22-c*). The second approach helps reduce the pH indicator strips needed and provides a more continuous pH profile. pH indicator strips with a range of pH 6-8 were used, as this is the target pH range of the system. pH indicator strips with a broader range of pH 1-11 were also used to check whether the pH had shifted beyond the desired range (*Figure 22-d*).

pH Distribution Accessed From the pH Indicator Stamp

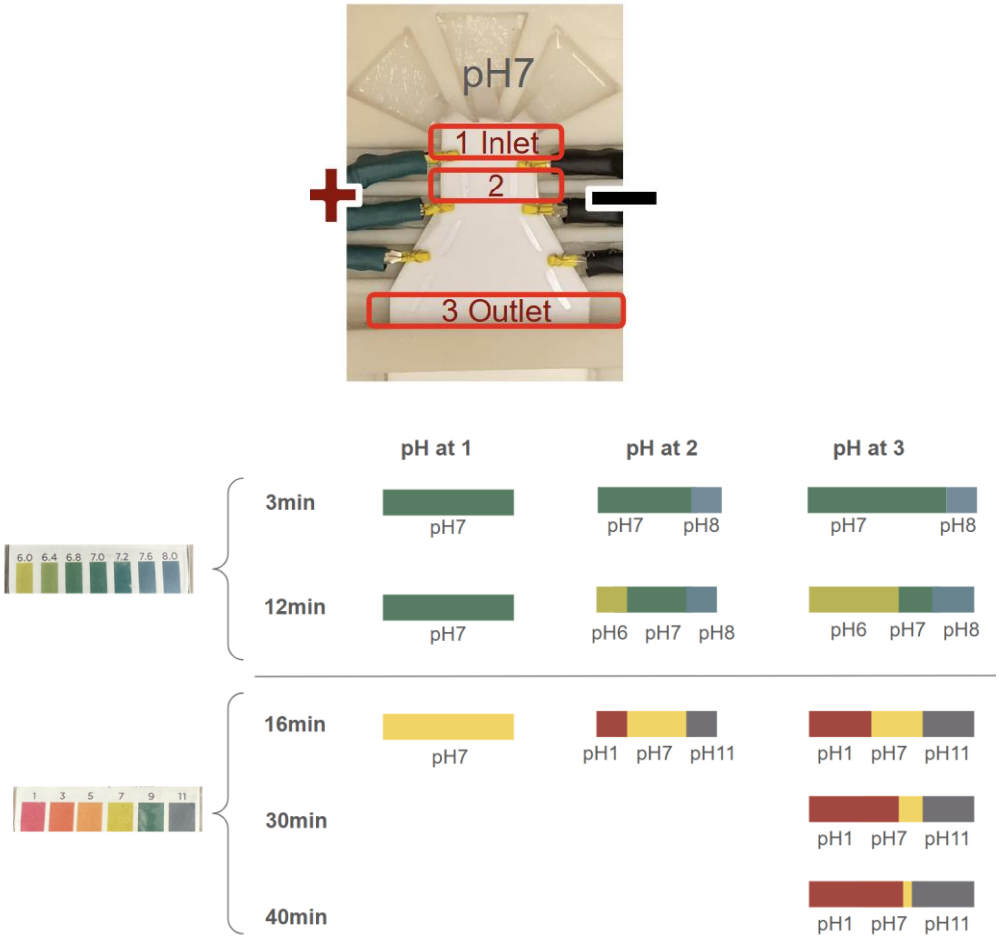

Figure 23: *pH distribution over time assessed using a pH indicator stamp. The image at the top shows the paper CFE setup, with three regions where the pH was measured: (1) inlet, (2) middle*

zone, and (3) outlet. A voltage was applied across the separation bed, and pH values were measured at the three regions over time. The pH color changes were interpreted using two pH indicator strips with different ranges (pH 6–8 and pH 1–11). Time points include 3, 12, 16, 30, and 40 minutes. The initial pH value from the buffer inlet was set to be pH 7. The pH values shown are visual estimations based on comparison with the indicator strip color charts and were referenced against buffer standards whose pH was verified with a pH meter. (Condition: Buffer + Electrolytes:100 mM ACES (pH 7) + 500 mM NaCl, 10 V (10-15 mA)).

After several rounds of design and setup iterations, significant pH shifts were observed due to the hydrolysis of the buffer near the electrodes. In *Figure 23*, the pH profiles at three positions were measured during the run at various time points. The initial pH was 7, and the buffering range of ACES is pH 6.1-7.5 [59]. The pH at positions 2 and 3 began to shift toward a more basic range near the negative electrode. By 12 minutes, the solution near the positive electrode started becoming more acidic. At 16 minutes, pH indicator strips with a broader range were used, revealing abrupt color changes from pH 1 to pH 7 to pH 11. Over time, the acidic and basic regions extended toward the center, compressing the neutral zone. By 40 minutes, only a thin region remained at pH 7. These results indicate that the pH is highly unstable, even under a low voltage of 10 V, and that the acidic and basic fronts from the electrodes gradually compress the neutral region, even in a flowing system.

Improving pH Stability by Reducing Salt Concentration

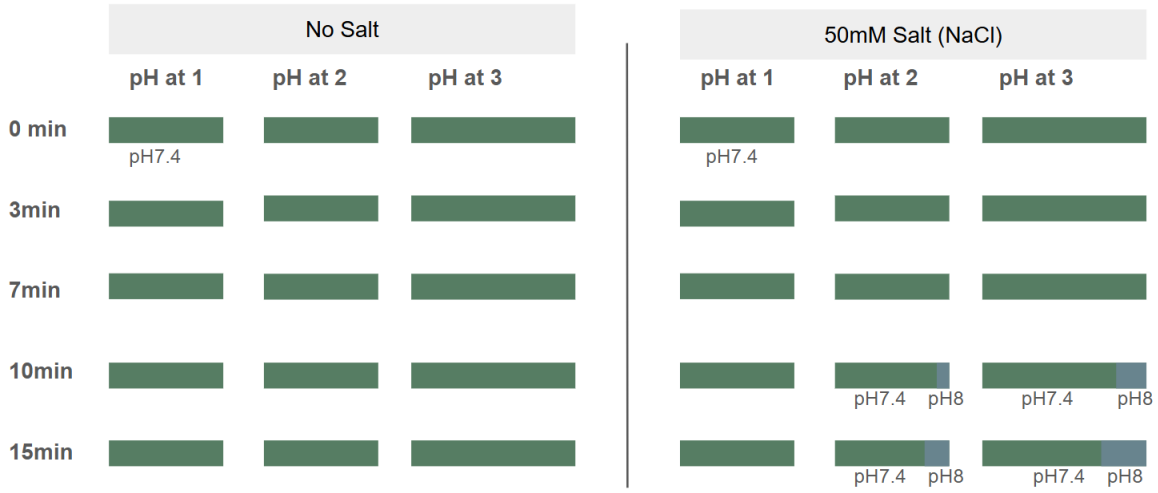

Figure24: *Effect of salt concentration on pH stability during paper CFE. pH was measured at three positions (1: inlet, 2: middle, 3: outlet) over time (as described in Figure 23) under two conditions: no added salt (left) and with 50 mM NaCl (right), with the initial pH from buffer inlet set as pH 7.4. (Condition: 10 mM histidine buffer pH 7.4 (+50 mM NaCl), 30 V, 0.02 A).*

In further experiments, it was found that removing salt from the system allowed the pH to remain stable for at least 15 minutes under 30 V. *Figure 24* shows a comparison of pH distribution changes over time between no salt and 50 mM salt conditions at 30 V. The buffering agent used was 10 mM histidine buffer, which has a buffering range of pH 5.5 to 7.4 [61]. The initial buffer pH was set to 7.4. The results show that under the no-salt condition, the pH remained unchanged throughout the 15-minute run. In the 50 mM salt condition, the region near the negative electrode became slightly more basic. This could be due to the initial pH being set near the upper end of the buffer's effective range. However, since the run duration is only about 10-15 minutes, this minor shift is acceptable. Although there is salt present in blood at approximately at the level of 150 mM [66], it will be diluted during the sample preparation process to lyse red blood cells and release

hemoglobin. A common way is using ammonium-chloride-potassium (ACK) buffer with 1:10 dilution factors in 1x ACK [67]. Moreover, the sample volume is small compared to the running buffer volume, so the salt concentration in the entire system will be further reduced. Therefore, the salt introduced from biological samples is not a significant concern in this context.

Issue Observed with No Salt Condition

Attempts were made to separate two proteins with a relatively larger IEP difference, mCherry (IEP = 5.63) and HbA (IEP = 6.91), under no- or low-salt conditions. However, no clear separation was achieved, and the migration behavior remained inconsistent. In some trials, one or both proteins exhibited migration under the electric field, while in others, no noticeable movement was observed. To troubleshoot this, a simplified 1D zone electrophoresis system was built to eliminate one spatial dimension and examine the horizontal migration behavior of the proteins.

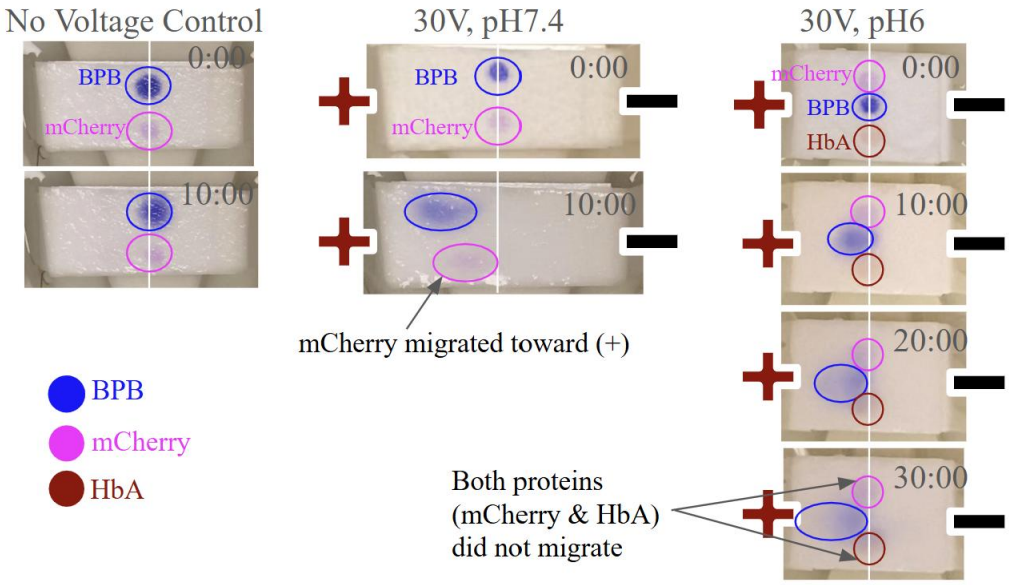

Figure 25: *Migration behavior of BPB, mCherry, and HbA under 1D paper electrophoresis at 30 V (0.02 A) using 10 mM histidine buffer at different pH conditions. The separation bed is 2 cm wide.*

1D electrophoresis tests were conducted using buffers at different pH levels. A 2 cm wide separation bed was connected to electrodes at each end using a curtain and tank cassette. No fluid flow was present in this setup. A control test without applied voltage (*Figure 25, left*) was conducted to ensure that any observed migration in other conditions was not due to uneven contact or setup bias. BPB was included as a tracer to confirm that the electric field was applied successfully. Under the condition of 30 V at pH 7.4, BPB and mCherry were loaded at the center of the separation bed, as indicated by the vertical white line (*Figure 25, middle*). Under 30 V at pH 6, mCherry, BPB, and HbA were similarly loaded at the center (*Figure 25, right*). Since pH 6 lies between the IEPs of mCherry and HbA, it was expected that they would migrate in opposite directions: mCherry toward the positive electrode and HbA toward the negative electrode.

The results showed that mCherry migrated toward the positive electrode at pH 7.4 but did not move at pH 6. HbA (IEP = 6.91), was expected to migrate toward the negative electrode but also did not move. These results suggest two possible explanations: either the pH was too close to each protein's IEP to induce sufficient net charge for migration, or non-electrophoretic factors, such as interactions with the paper, were interfering with movement. To differentiate between these possibilities, simple flow experiments were performed across a range of pH conditions, revealing potential issues with protein precipitation and adhesion to the paper at low salt condition (see Chapter 3.6 for details). Also, earlier experiments (Chapter 4.2) confirmed that the electric field was strong enough to mobilize proteins under 30 V, as shown by protein focusing in the FFFSE setup (high salt condition).

Discussion

This chapter investigates different buffer systems for protein separation on a miniaturized paper CFE platform. By testing single buffer, discontinuous buffer, FFFSE systems, and pH gradient, we investigate how parameters like electric field strength, pH environment, pH stability, and paper–analytes interactions influence separation behavior.

In the single buffer system, no separation was observed between HbA and HbS, even when the buffer pH was set between their IEPs. While the compression of the pH from the electrodes under high-salt conditions may have contributed to this outcome, it also suggests that the difference in electrophoretic mobility between these two proteins may be too small to resolve under the current scale, time, and voltage settings. Although hemoglobin variants could not be separated under this condition, the experiments successfully demonstrated that protein migration direction can be controlled by tuning the surrounding pH relative to the IEP. A future direction involving the use of an additional binder to exaggerate the IEP differences of HbA and HbS is introduced in Chapter 5.

The discontinuous buffer system offered an obvious improvement in spatial resolution by utilizing the principle of IEF. Compared to the single buffer system, focusing and more distinct separation of BPB and hemoglobin were observed. However, the system was unable to achieve separation between Hb variants, suggesting that sharper and more stable pH steps are needed to resolve proteins with closely spaced IEPs. Therefore, a three-zone buffer design was proposed and tested, aimed at forming pH interfaces to target proteins with specific IEP differences. Utilizing a stepwise pH gradient, rather than a continuous gradient, may improve spatial resolution and produce sharper focusing at the pH interfaces. This strategy would require precise pH control and

stability. However, hydrolysis at the electrodes and ionic movement introduced instability in the pH gradient.

FFFSE was tested as a strategy to enhance field strength at the center of the separation bed without increasing overall voltage. The project proceeded with the discontinuous buffer system, as the initial goal was to determine the pH and buffer composition that could enable separation of HbA and HbS. Voltage reduction was considered a secondary objective to be addressed afterward. Therefore, FFFSE remains a potential method to enhance separation and could be considered in future studies with further investigation.

During troubleshooting, pH instability was identified as a major factor limiting separation performance. It was found that removing salt from the system helped stabilize the pH for at least 15 minutes under 30V, which is promising for short duration runs. However, under no-salt conditions, new challenges appeared. Protein migration became inconsistent, and increased adhesion to the paper was observed. 1D electrophoresis experiment with mCherry and HbA showed that under conditions where opposite migration directions were expected, the proteins failed to move toward either electrode. And the flow test described in Chapter 3.6 suggests that protein solubility and protein-paper interactions become more problematic at low ionic strength, particularly when pH is close to the protein's IEP. Overall, we want to avoid high salt concentrations due to pH instability and the potential for salting-out effects. The salt from the blood sample is not a major concern, as it will be diluted during the sample preparation step. Additionally, the sample loading volume is small compared to the total running buffer volume, which further reduces the salt concentration to a level that is unlikely to affect pH stability within our desired run time. However, low-salt conditions also raise issues such as protein precipitation and adhesion to the paper as discussed in Chapter 3.6.

These issues reduced the suitability of the chosen paper material. While Grade 691 performed well in early flow tests due to its clean migration behavior, its glass fiber composition and negatively charged surface likely contributed to protein adhesion under low-salt or neutral to basic conditions. Surface blocking with BSA and Tween 20 provided slight improvement in protein flow, but noticeable tailing behind the migration path was still observed. This suggests that Grade 691 may not be ideal for low-salt protein separation applications. Selecting new paper material may help resolve this limitation (see Chapter 5.1 for details).

4.5 Assessing Quantification Capability on Paper

Although separation of two proteins was not achieved in previous experiments, we still aimed to access the ability the device's ability to perform quantitative analysis of Hb concentration. Quantitative results are important for identifying heterozygous status, monitor disease severity, and track treatment response. Typically, in SCT heterozygous individuals, HbS level range 20% to 40%, while in SCD homozygous individuals they often approach 100% [37] [68]. In transfusion therapy, the goal is to reduce the HbS level to < 30 % [9]. Additionally, although this prototype does not focus on HbF, hydroxyurea treatment has been shown to be effective when HbF concentrations are raised to 30 % [69]. Therefore, it is crucial to determine whether this platform can perform quantitative results to distinguish these clinically relevant differences.

To evaluate this, a flow test was conducted using different concentrations. Flow patterns were recorded, and the intensity was quantified to assess correlation with Hb concentration. HbA was initially resuspended in 1x PBS at a concentration of 15 g/L, corresponding to 0.1x the total Hb concentration typical found in homozygous or heterozygous samples (~150 g/L) [18]. This dilution is performed because, in practical applications, the blood must first be diluted to lyse red blood cells (see Chapter 5.5 for details). PBS was used to resemble the physiological condition of

blood. After that, 0.1x HbA solution was further diluted with water to 0.05x, 0.02x, and 0.01x concentrations. Taking 0.1x as 100 % Hb concentration, the resulting concentrations of 0.05x, 0.02x, and 0.01x correspond to 50 % (7.5 g/L), 20 % (3 g/L), and 10 % (1.5 g/L), respectively. These concentrations of HbA were then physically loaded onto the test strip at separate locations (*Figure 26-a*).

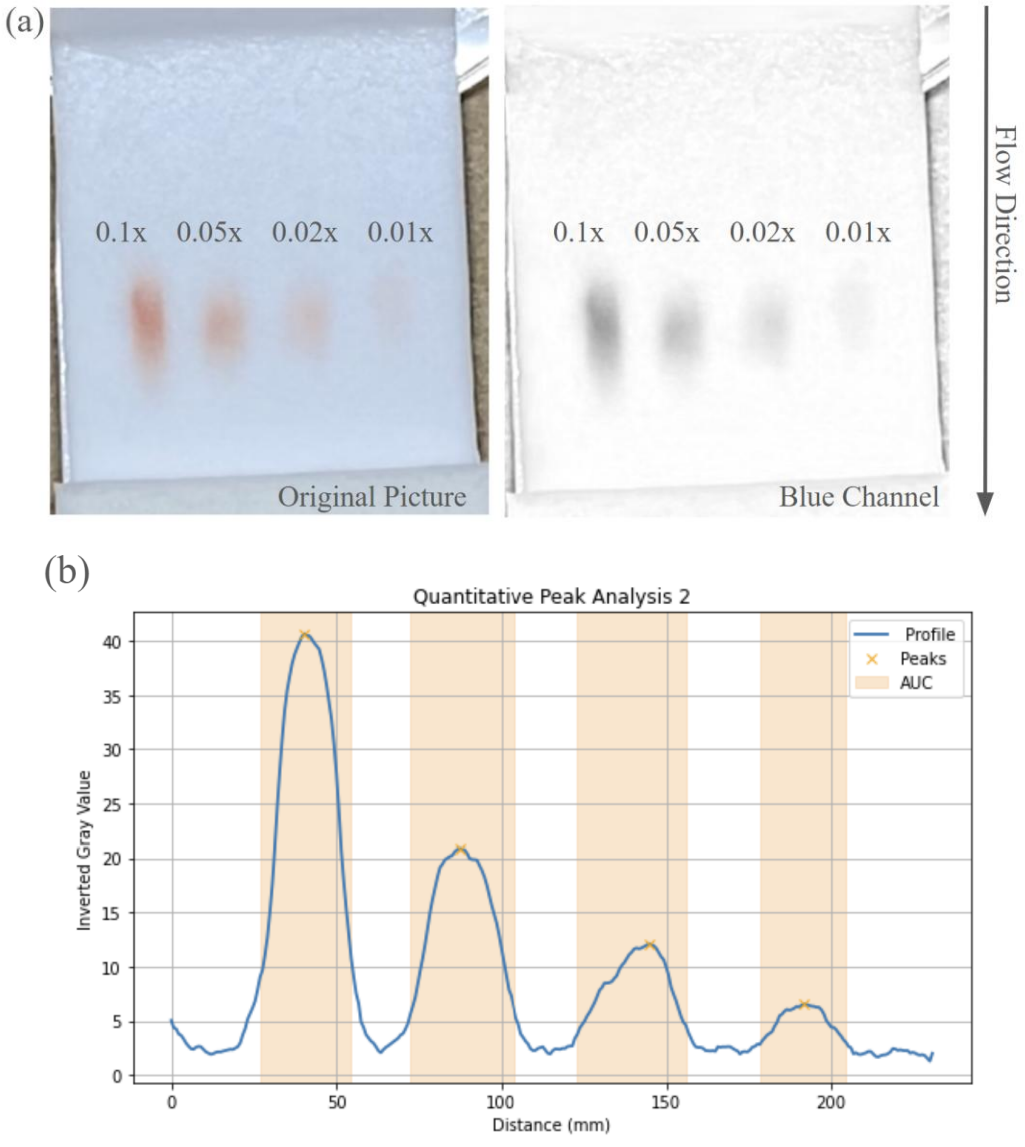

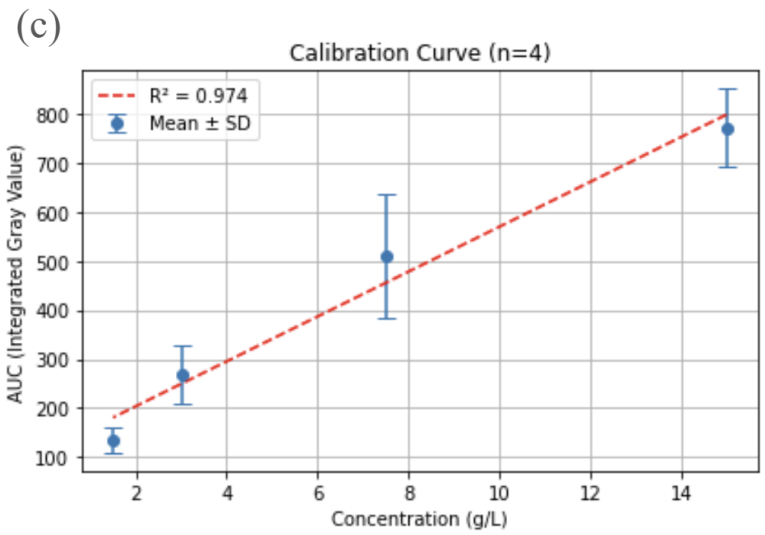

Figure 26: *Evaluating the quantification capability of the platform (a) Image captured during the flow test (left), with the blue channel extracted for analysis (right). 1 µL HbA at different concentrations were loaded on the paper at different position. (b) Quantification of intensity in inverted gray values along the horizontal distance of the strip. Note: The analysis method follows that described in Chapter 4.2; only the grayscale was inverted here for more intuitive interpretation. Higher values indicate darker color. (c) Calibration curve (n = 4), plotting area under the curve (AUC) of gray values against Hb concentration. p = 2.83 x 10^{-6}. Concentration levels: 1.5 g/L = 0.01x = 10 %, 3 g/L = 0.02x= 20 %, 7.5 g/L = 0.05x = 50 %, 15 g/L = 0.1x = 100 %.*

As shown in *Figure 26-b* and *26-c*, the signal from each HbA concentration was quantified by the area under curve (AUC). The AUC increased linearly with HbA concentration, with R^2 = 0.974. One way ANOVA showed a significant difference between groups (p = 2.83 x 10^{-6}). This confirms that AUC values are statistically significantly different across concentrations. These results support a strong correlation between signal intensity and Hb level. They also show that Hb on paper can be quantified. Clinically relevant differences can also be clearly distinguished.

4.6 Overall Discussion and Conclusion

This project aimed to develop a miniaturized paper CFE platform with hemoglobin variants as analytes. The long-term goal is to develop an accessible diagnostics tool for SCD. Although complete separation between HbA and HbS was not achieved, meaningful progress was made across several key areas, providing a foundation for future development.

One of the strengths of this platform is its ability to control fluid flow by capillary-driven flow without the need for external pumps or gravity-driven flow, making it a promising candidate for POC applications. Paper geometry and setup designs led to a platform where sample input, electric field exposure, and buffer environments can be independently controlled. This flexibility is important for expanding the platform toward more complex design such as multi-zone pH control.

Three buffer systems were tested to evaluate their effectiveness in separating proteins based on their electrophoretic mobility and IEP. The experiments confirmed that protein migration direction could be controlled by tuning the surrounding pH (in single buffer system when the difference between pH and IEP is around 0.3~0.5). Among them, the discontinuous buffer system showed improved resolution between analytes, and the combination of discontinuous buffer and FFFSE further demonstrated sharper focusing of the proteins. These results support the principle that pH-based separation is possible on this platform. However, maintaining a stable and well-defined pH environment remained one of the main technical challenges. Hydrolysis at the electrodes and ion movement in the electric field disrupted the built pH gradients, even under low voltage (10 V) conditions. pH indicator stamping experiments showed dramatic pH shifts over time and compressing of the neutral zone. To address this, salt was removed from the system, which helped maintain pH stability for at least 15 minutes under 30 V. While this was promising

for short runs, removing salt also caused new problems, such as protein precipitation and adhesion to the paper, especially when pH was close to the protein's IEP. This result found the core tradeoff in the system. High salt leads to pH instability and may cause salting out. On the other hand, low salt improves pH control but increases the chance of protein precipitation and adhesion. Since the pH control is the key of this platform, changing paper material is suggested to solve this tradeoff. It is also important to select a buffering agent with high ERC to maintain pH distribution stability, and with a buffering range that covers the target pH gradient. A combination of buffering agents may be used to create a broader pH gradient or to form sharper pH steps. Based on the migration of proteins under both high salt and low salt conditions in the electric field, the IEP difference between HbA and HbS (ΔIEP ~0.3) may not be large enough to separate them under the current running time and voltage. However, their electrophoretic mobility is sufficient for them to deflect toward the electrodes with this platform size when the surrounding pH is farther from their IEP. Therefore, to achieve separation, we may consider increasing the running time. In the traditional IEF protocol for hemoglobin IEF, the voltage*hour value is usually set to 550vh in the separation phase across 5 cm IEF gel [24]. Another option is to design a longer neck, where the electrodes are placed closer together, allowing the proteins to pass through an area with stronger electric field for a longer time. Increasing the voltage could also reduce the required time, but we want to avoid that since the final goal is to power the system using a simple battery. Another strategy would be to exaggerate the IEP difference between HbA and HbS, which will be discussed in Chapter 5.

Another valuable outcome was the successful quantification of hemoglobin concentration using the platform. AUC from the signal intensity showed a strong linear relationship with hemoglobin concentration across a clinically relevant range, and statistically significant differences between the concentrations were observed.

In conclusion, this thesis demonstrates the development of a low cost, paper based, miniaturized platform for CFE. The system successfully showed separation between dye and protein. Although full separation between HbA and HbS was not achieved, the results suggest that it is still possible with improved system design and further testing. The experiments confirmed that the direction of protein migration can still be controlled by adjusting the pH relative to each protein's IEP. Throughout this work, pH stability was identified as a key factor in separation performance. Using appropriate buffering agents and lowering salt concentration helped stabilize the pH for at least 15 minutes under 30 V, which is suitable for short diagnostic runs. However, reducing salt also caused problems with protein solubility and increased protein adhesion to the paper surface. This suggests that material choice plays a major role, and changing to a different paper with lower protein-paper interaction could improve results under low salt conditions. The hypothesis is considered feasible for cases with larger ΔIEP, though careful material selection is needed to minimize protein-paper interactions under varying pH conditions. For cases with small ΔIEP, compromises may need to be made to enhance separation, such as increasing field exposure time or field strength by reducing separation distance or increasing voltage. Overall, this project provides a foundation for future work toward miniaturizing paper CFE for expanding accessibility of electrophoresis for protein separation.

CH5 Future Directions

5.1 Paper Material Selection and Geometry Considerations

Protein-Paper Interaction

Although this project successfully demonstrated the separation of dye and protein and showed that hemoglobin variants can move in different directions, there are still some problems that need to be solved. One major unsolved issue is the tradeoff between maintaining a stable pH gradient, optimizing salt concentration, and reducing the unwanted interactions between proteins and the paper material. As discussed earlier, high salt conditions can lead to unstable pH due to ion migration and hydrolysis around electrodes. However, low salt conditions improve pH stability but increase protein adhesion and precipitation on the chosen testing paper. While flow tests with surface blocking and detergent helped improve protein migration, this approach adds complexity to the fabrication process and could potentially be avoided by choosing a more suitable paper material.

One solution is to change the paper material. Grade 691 is a glass fiber material with a negatively charged surface under a wide pH range, which tends to increase protein adhesion under low ionic strength or neutral/basic pH conditions. This makes it less ideal for protein separation. The Šlais group explored hydrophilized polypropylene non-woven fabrics for their DF-IEF on proteins, which may reduce protein sticking and improve flow behavior. A quick test using this material could be valuable. Paper materials with fewer available surface hydroxyl groups may be preferable, as they can reduce surface charge and minimize charge variation across different pH conditions.

In addition to properties like thermal stability, flow rate, and minimal dispersion, it was found that protein adhesion to some materials varies with pH. This makes pH-dependent adhesion an important parameter to evaluate when selecting a material for paper CFE systems. Since this platform relies on pH manipulation to control protein flow, the separation bed should minimize protein-paper interaction regardless of pH. Future tests should therefore evaluate materials at multiple pH levels using flow experiments.

Flowrate and Time Under Field

The separation between HbA and HbS was not achieved when the pH was set between their isoelectric points, suggesting that the time under the electric field was insufficient. To increase separation performance, future designs could:

- Reduce flow rate by selecting a separation bed with flower flow rate and/or a weaker absorbent pad.
- Increase the neck length where the electrodes are positioned closer together. This allows proteins to pass through a region with stronger field strength for a longer time, improving initial separation (*Figure 27*).

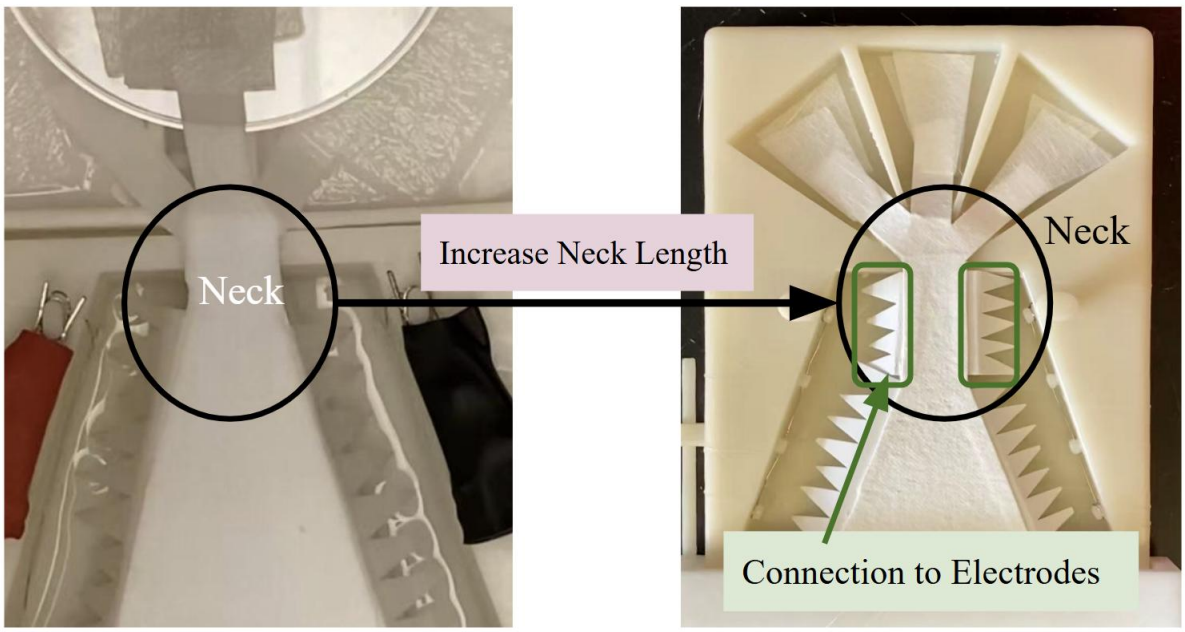

***Figure 27**: Paper geometry with longer neck area to connect electrodes and increase protein exposure time under electric field.*

5.2 Shifting Isoelectric Point to Enhance Separation

To improve separation of hemoglobin variants, researchers have developed strategies such as modifying their charge properties. In the HemeChip device used for detecting glycosylated hemoglobin for diabetes diagnostics, an affinity buffer that reacts with HbA was used, making it carry a more negative change. This increases the difference in electrophoretic mobility compared to glycohemoglobin (HbA1C), enhancing the separation [70]. This rationale could also be applied in this thesis to enhance separation of HbA and HbS. Unlike HemeChip, whose separation relies on electrophoretic mobility difference in zone electrophoresis, the proposed system uses the separation principle of IEF. Therefore, a potential strategy is to add a secondary binder that shifts the IEP of HbS further away from that of HbA. As introduced in Chapter 1, HbS has a higher IEP than HbA. Therefore, shifting the IEP of HbS to a higher value could exaggerate the difference of IEP between HBA and HbS. Below are some potential approaches to explore:

HbS-specific Antibodies

A readily available option is the use of commercially available HbS-specific antibodies. When the antibody binds to HbS, it can shift the IEP depending on the IEP of the antibody. However, antibodies are expensive, which would significantly increase the cost of the system. Therefore, they may not be ideal to use in the development of low-cost POC devices.

Synthetic Non-antibody Binders

Another option would be to utilize synthetic non-antibody binders as an alternative to conventional antibodies. These binders can be discovered through biopanning. The concept of biopanning involves screening and selecting a large pool of binders against the target antigen, in this case, HbS. The IEP of HbS can be shifted by attaching a protein with a different IEP. After binding, the protein-HbS complex will behave as a single unit under the electric field and migrate based on the combined IEP of the complex. Therefore, when discovering these binders, it is important not only to ensure high affinity and specificity to HbS, but also to consider whether the binding can shift the overall IEP of HbS in the desired direction. Addition to that, we can also engineer and fuse another protein onto the binder to further control the direction and magnitude of IEP shifting. By exaggerating the IEP difference between HbA and HbS, we can gain larger and faster spatial separation on the paper CFE platform.

The utilization of synthetic binders reduces both time and cost, and eliminates the need for the labor-intensive monoclonal antibody production processes involving animals. The biopanning process has also been greatly improved by using the phage-like particle (PLP)-based system developed by Kline et al. in the Lutz Lab [71]. This platform enables shorter processing times and simpler purification steps, making the technique more accessible. Compared to traditional phage

display, the synthetic PLP-based display of the binders allows for a greater variety of proteins to be presented, as it is not limited by self-replicating phage. It is also more cost-effective and easier to manufacture. To express these PLPs with the binders, the binder sequences would be cloned into a vector. A ligation-independent cloning method was used to speed up the cloning process. The vector with a ligation-independent cloning site was developed by Enos Kline in the Lutz Lab, where I assisted with experiments during its development.

5.3 In flow Reference: Engineering Reference Proteins as IEP Ladder

An attempt was made to manipulate IEPs through protein engineering, aiming to develop an IEP ladder that could be integrated into the flow system. This ladder could serve as a reference to indicate the IEPs of separated analytes. Since the pH gradient is invisible, incorporating reference proteins with known IEPs would allow tracking of the pH profile. Because of potential fluid flow bias in the system, such as uneven contact between absorbent pads and the testing paper or slight tilting of the cassette, it is difficult to predict the exact positions where HbA and HbS will migrate. By using reference proteins as an IEP ladder, the identity of separated analytes can be determined based on their relative positions. This ladder can also serve as an intensity reference to help estimate hemoglobin concentration for quantification.

Seven reference protein with IEP values of 6.81, 7.00, 7.10, 7.30, 7.39, 7.80, and 8.30 were engineered by adding a tag on EGFP to shift its net IEP (*Figure 28*). EGFP was chosen because it is a fluorescent protein that can be seen by eye. By modifying EGFP to have different IEP values, it can become a practical visual tool for confirming separation and providing reference points within the system.

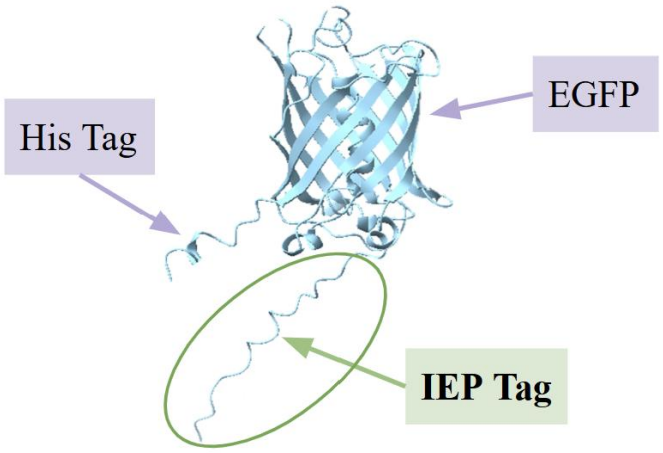

***Figure 28**: The molecular structure of EGFP with a His tag for protein purification and an IEP tag for isoelectric point shifting. (Molecular graphics and analyses were performed with UCSF ChimeraX.)*

The IEP tag was added to EGFP through site directed mutagenesis using an insertion method. The tag sequence was inserted into the plasmid containing EGFP using exponential amplification with Q5 Hot Start Enzyme, which amplified and linearized the plasmid [72] [73]. Then, the KLD enzyme mix, which contained kinase, ligase, and DpnI, was used to phosphorylate, ligate, and remove the original template, making the plasmid circular again. The modified EGFP was then expressed using an *E. coli* system.

However, it was found that the green fluorescence of EGFP is difficult to see on white paper, even under UV light. This makes it a less ideal option for visual markers in this system. The IEP values of the modified proteins still need to be verified using traditional IEF methods, but the lab currently lacks the materials and equipment for that. Future work could focus on verifying the IEP values and improving the visibility of the reference proteins before fully integrating the ladder into the paper CFE system.

5.4 Electrode Material and Design Optimization

In early experiments using a common alligator clip as the electrode, colored streaks were observed downstream of the positive electrode, as shown in *Figure 29*. This was likely caused by corrosion or metal ions leaching when voltage was applied, which is an unwanted side effect. The exact material of the alligator clip is unclear, as it was a shared item in the lab. However, the orange, brown, and black streaks were suspected to be metal oxides such as iron (orange), or copper (green or black) [74]. This issue was resolved by replacing the electrode with a platinum wire, which is inert and resistant to oxidation and corrosion. This observation shows the importance of electrode material selection in the system. Although platinum successfully prevented corrosion, it is expensive and may limit the accessibility of this system for POC applications. Therefore, identifying a cheaper but still inert electrode material is a desirable direction for future development.

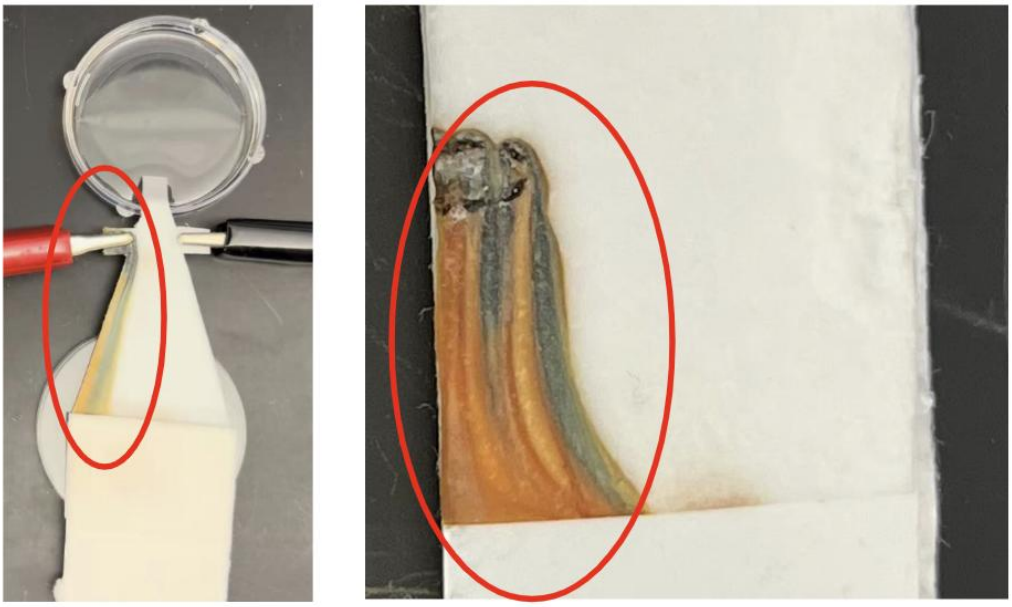

Figure 29*: Colored streaks suggesting corrosion downstream of the alligator clip electrode.*

Another issue observed during testing was the overheating of the paper when applying 50 V with the electrode in direct contact with the paper. In some cases, visible smoke was produced, indicating localized burning. This problem motivated the development of the tank cassette, which separates the electrodes from the paper. However, to move forward with developing a POC device, we aim to eliminate the need for the tank setup.

The smoking and burning issues are likely to result from multiple factors. One is localized heating due to the small contact area between the clip electrode and the paper, which leads to high current density at that point. In addition, regions with higher resistance, possibly due to drying or bubble formation, convert more electrical energy into heat. Poor contact between the electrode and the paper can also increase resistance at the connection point. This creates a cycle: poor contact or localized contact lead to high current density and localized heating, the heating dries out the paper, which further increases the resistance and cause more heating, eventually resulting in paper smoking or burning. To address this issue, several desirable conditions were considered:

- Flatten and increase contact area: Ensure a broader, more even electrical connection to prevent high current density and high resistance points.
- Ensure good electrical contact: To help reduce resistance.
- Maintain fluid near the electrode: To prevent drying.

One attempt to solve this involved adding an extra layer of the testing paper between the clip and the paper (*Figure 30*). The rationale was to increase the liquid volume at the contact site to prevent drying and burning. However, this approach was not successful, as smoking was still observed when applying 50 V.

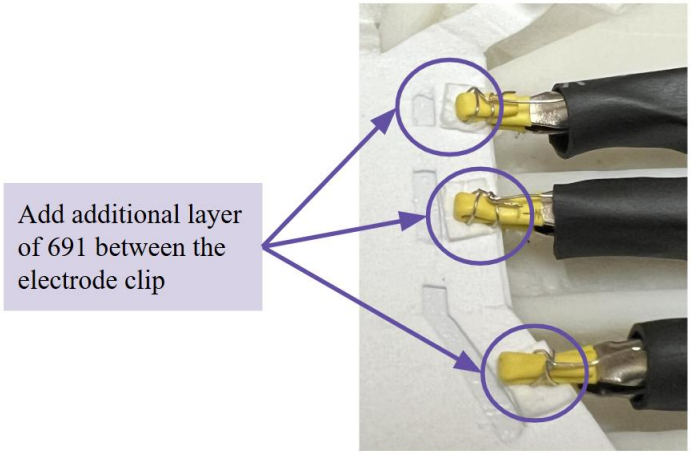

***Figure 30**: Image showing the additional layer of Grade 691 paper inserted between the electrode clip and the testing paper.*

Although the use of platinum wire and the tank cassette were effective in a lab setting, they are not suitable for a final POC device due to their high cost and lack of portability. For the development of a practical POC system, the electrode material and configuration must meet some key requirements, such as being cost-effective and disposable. The electrodes should be inexpensive, easy to manufacture, designed for single use, and embedded directly onto the testing paper. Alternatively, if no sufficiently stable and low-cost disposable material is available, more durable material can be embedded in a reusable cassette. Additionally, the geometry of the electrodes should be considered. As discussed earlier, longer electrode contact with the separation bed is desirable, not only to prevent localized heating but also to extend the time analytes spend under the electric field, which can improve separation performance.

A proposed solution is to use carbon conductive ink as the electrodes. It can be printed directly onto the paper and is chemically stable [75]. By printing the carbon ink along the edge of the separation bed, a longer electrode contact area can be achieved. This approach is cost-effective

and suitable for disposable POC applications. However, one potential concern is the conductivity of the carbon ink, which may require further evaluation.

5.5 Upstream Sample Preparation

Currently, the system uses mimic samples of HbA and HbS prepared in PBS. To transition toward practical use, upstream sample preparation from whole blood is required. The desired characteristics of the sample preparation process include minimal processing steps, low cost, and environmentally friendly.

A potential option for red blood cell lysis is the use of distilled water, which utilizes osmotic pressure. When whole blood is diluted in a hypotonic environment, such as water, the lower external salt concentration causes water to flow into the cells. This results in membrane rupture and the release of hemoglobin. This method is simple, low-cost, and environmentally friendly. However, a potential drawback is the required blood-to-water ratio for effective lysis. If over-diluted, the visibility of hemoglobin variants on the paper CFE system may be reduced, thereby limiting detection and interpretation. In HemoType SC, a 1:1000 dilution was used to lyse red blood cells [18]. Future work may involve determining the minimal effective dilution ratio to balance lysis efficiency and detection sensitivity.

Another commonly used method is lysis with ACK buffer, which is also effective for red blood cell lysis. The typical volume ratio is 10:1 of 1x ACK buffer to whole blood [67]. This level of dilution is comparable to that used in Chapter 4.5 for quantitative analysis, which is favorable. However, one concern is that the salt in the ACK buffer may affect pH stability in the separation process. This effect will need to be evaluated in future testing.

5.6 Downstream Data analysis Method

To enable POC application, the result output must be easy to interpret by untrained personnel. Therefore, developing a simple and automated data analysis method is important. Visual detection through color separation is the most straightforward method. Also, with an intensity analysis method, the platform has the potential to provide quantitative results. In cases where color contrast is insufficient, illumination at 410 nm could be applied, where hemoglobin exhibits stronger absorbance [32]. This is used in Gazelle Hb Varient system to improve detection of weak signals. Future development may also involve integrating smartphone-based image capture and automated interpretation algorithms to enhance accessibility and standardization.

5.7 Power Source Integration

Currently, the system operates using a benchtop power supply. For the POC device, integration of a battery-powered setup is essential. Experimental results have demonstrated that hemoglobin migration is achievable under 30-50 V, which is a voltage level that can be supplied by a battery system. Based on the measured current on the developed platform and tested buffer composition, the low salt condition usually has the current of 15 mA to 20 mA. These indicate a promising direction for future integration, enabling a fully portable and low-power POC device.

Appendix 1: Other Paper Geometries Explored

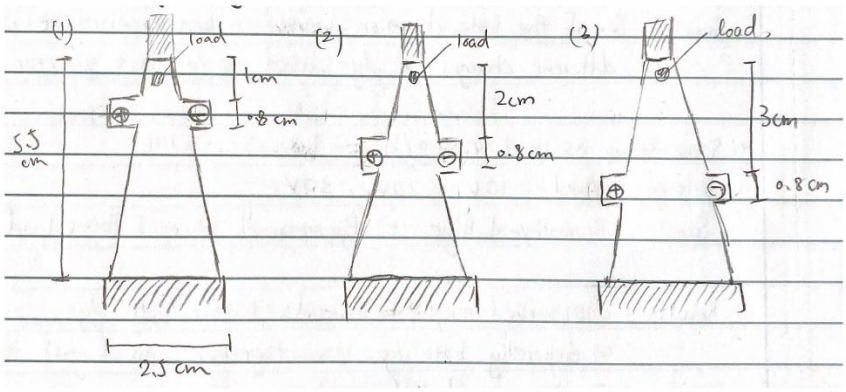

Appendix1 Figure 1*: Paper Geometry with Electrode Placed at different positions. (Notebook Draft: Hand-drawn sketches of different paper geometries tested in early prototyping)*

The effect of placing electrodes at different positions along the flow path was investigated. The results support the conclusion that a single pair of electrodes is insufficient. As discussed in the main chapter, a longer electrode connection is desirable to increase the duration under the electric field and to reduce heating.

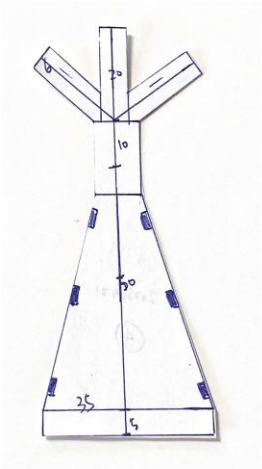

Appendix 1 Figure 2*: Paper Geometry with three buffer inlet, 1 cm neck, and 5 cm long separation bed. (Notebook Draft: Hand-drawn sketches of paper geometry)*

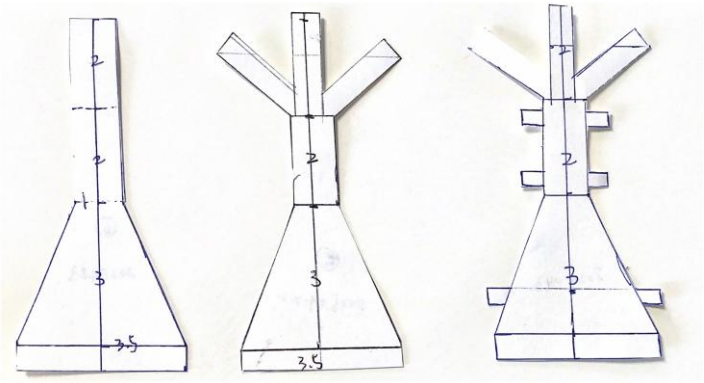

Appendix 1 Figure 3*: Paper Geometries for single buffer system and three inlet discontinuous buffer system. The neck was extended from 1 cm to 2 cm to increase time under field, and the separation bed length was decreased from 5 cm to 3 cm. The right-most geometry is for clip electrode, while the left one and the middle one is for tank cassette setup (Notebook Draft: Hand-drawn sketches of paper geometry)*

Appendix 1 Figure 4*: A picture of the setup drawn in Appendix1 Figure3 (middle), with the electrode curtain attached.*

An attempt was made to use a paper geometry with a longer neck to increase the analytes' exposure time under a stronger electric field. However, due to unresolved issues with adhesion to the paper, no flow or separation was achieved.

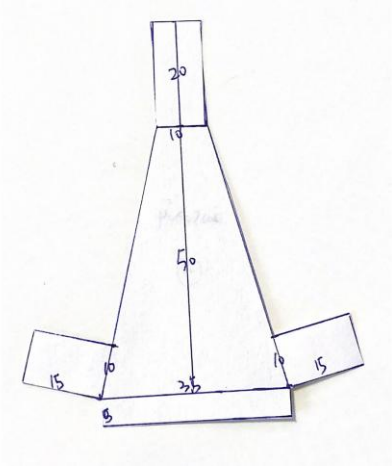

Appendix 1 Figure 5: *Paper geometries exploring the use of the same material as both the testing paper and the electrode curtain. (Notebook Draft: Hand-drawn sketches of paper geometry)*

Appendix 1 Figure 6: *A picture of the flow test with color dye on the geometry shown in Appendix 1 Figure5.*

This flow test indicates that, to minimize flow from the curtain, which is compressing the running buffer flow in between the curtain, a material with a slower flow rate than the testing paper is preferred.

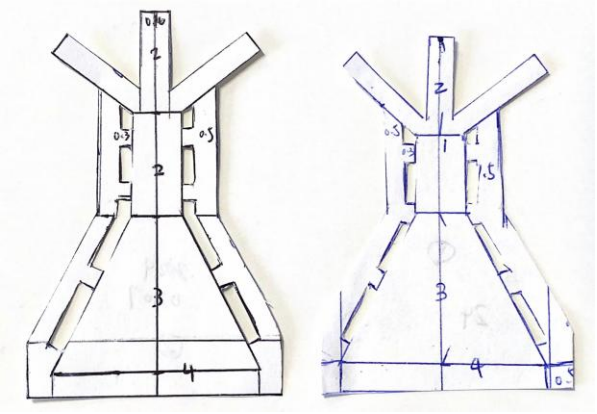

Appendix 1 Figure 7: *Paper geometries explored to address hydrolysis issues introduced by the electrodes, with slight variations in the position of the bridge connecting to the separation bed. (Notebook Draft: Hand-drawn sketches of paper geometry)*

Appendix 1 Figure 8: *A picture of the flow test with color dye on the geometry shown in Appendix 1 Figure7. (No voltage was applied)*

A separate flow channel for the electrodes was introduced in hopes that the pH-altered buffer, resulting from hydrolysis at the electrodes, could be flushed away in that channel and would not affect the pH in the separation bed. However, the results showed that this strategy did not work.

Appendix 2: Python Code for Intensity Quantification Analysis

[Code generated with assistance from OpenAI's ChatGPT]

```
import pandas as pd
import numpy as np
import matplotlib.pyplot as plt
import glob
import os
from scipy.integrate import trapz
from scipy.signal import find_peaks, peak_widths
from sklearn.linear_model import LinearRegression
from sklearn.metrics import r2_score
from scipy.stats import f_oneway

# path to CSV folder
folder_path = r"(insert folder path)"
csv_files = sorted(glob.glob(os.path.join(folder_path, "*.csv")))

# Create a list to store AUCs
all_auc = []

for file in csv_files:
    data = pd.read_csv(file, header=None, skiprows=1)
    x = data[0].astype(float).to_numpy()
    y = data[1].astype(float).to_numpy()

    peaks, _ = find_peaks(y, height=2.5, distance=50)
```

```
    widths = peak_widths(y, peaks, rel_height=0.8)

    filename = os.path.basename(file)
    plt.figure(figsize=(8, 5))
    plt.title(f"{filename.replace('.csv', '')}")
    plt.plot(x, y, label=' Profile', linewidth=1.8)
    plt.plot(x[peaks], y[peaks], 'x', color='orange', label='Peaks')

    for i in range(len(peaks)):
        left = int(widths[2][i])
        right = int(widths[3][i])
        auc = trapz(y[left:right+1], x[left:right+1])
        all_auc.append(auc)
        plt.axvspan(x[left], x[right], color='#FFCC99', alpha=0.5, label='AUC' if i == 0 else "")

    plt.xlabel("Distance (mm)")
    plt.ylabel("Inverted Gray Value")
    plt.grid(True)
    plt.legend()
    plt.tight_layout()
    plt.show()

print("Total number of AUCs read:", len(all_auc))

# Reshape AUCs to [concentration x replicates], 4 concentrations with 4 replicates each
peak_aucs_array = np.array(all_auc).reshape(4, 4).T
print(peak_aucs_array)
```

```
# Means and standard deviations
auc_means = np.mean(peak_aucs_array, axis=1)
auc_stds = np.std(peak_aucs_array, axis=1)

#Define concentrations (must match order of reshaped AUC matrix)
concentrations = np.array([15, 7.5, 3, 1.5])  # g/L
X = concentrations.reshape(-1, 1)
y = auc_means



# Linear regression
model = LinearRegression()
model.fit(X, y)
y_pred = model.predict(X)
slope = model.coef_[0]
intercept = model.intercept_
r2 = r2_score(y, y_pred)

print(f"Regression equation: AUC = {slope:.2f} x Concentration  + {intercept:.2f}")
print(f"R² = {r2:.4f}")

# Plot calibration curve with error bars
plt.errorbar(concentrations, auc_means, yerr=auc_stds, fmt='o', capsize=5, label='Mean ± SD')
plt.plot(concentrations, y_pred, 'r--', label=f'R² = {r2:.3f}')
plt.xlabel("Concentration (g/L)")
plt.ylabel("AUC (Integrated Gray Value)")
```

```
plt.title("Calibration Curve (n=4)")
plt.grid(True)
plt.legend()
plt.tight_layout()
plt.show()

# One-way ANOVA
conc1 = peak_aucs_array [0, :]
conc2 = peak_aucs_array [1, :]
conc3 = peak_aucs_array [2, :]
conc4 = peak_aucs_array [3, :]

F_statistic, p_value = f_oneway(conc1, conc2, conc3, conc4)
print("ANOVA result:")
print("F =", F_statistic)
print("p =", p_value)
```

References

[1] "Sickle Cell Disease - What Is Sickle Cell Disease? | NHLBI, NIH." Accessed: May 10, 2025. [Online]. Available: https://www.nhlbi.nih.gov/health/sickle-cell-disease

[2] A. M. Thomson *et al.*, "Global, regional, and national prevalence and mortality burden of sickle cell disease, 2000–2021: a systematic analysis from the Global Burden of Disease Study 2021," *The Lancet Haematology*, vol. 10, no. 8, pp. e585–e599, Aug. 2023, doi: 10.1016/S2352-3026(23)00118-7.

[3] K. Esoh and A. Wonkam, "Evolutionary history of sickle-cell mutation: implications for global genetic medicine," *Human Molecular Genetics*, vol. 30, no. R1, pp. R119–R128, Apr. 2021, doi: 10.1093/hmg/ddab004.

[4] CDC, "Data and Statistics on Sickle Cell Disease," Sickle Cell Disease (SCD). Accessed: May 10, 2025. [Online]. Available: https://www.cdc.gov/sickle-cell/data/index.html

[5] M. H. Steinberg and P. Sebastiani, "Genetic modifiers of sickle cell disease," *American J Hematol*, vol. 87, no. 8, pp. 795–803, Aug. 2012, doi: 10.1002/ajh.23232.

[6] M. J. Stuart and R. L. Nagel, "Sickle-cell disease," *The Lancet*, vol. 364, no. 9442, pp. 1343–1360, Oct. 2004, doi: 10.1016/s0140-6736(04)17192-4.

[7] S. Lanzkron, C. P. Carroll, and C. Haywood, "The burden of emergency department use for sickle-cell disease: An analysis of the national emergency department sample database," *American J Hematol*, vol. 85, no. 10, pp. 797–799, Oct. 2010, doi: 10.1002/ajh.21807.

[8] "Sickle Cell Disease - How Sickle Cell Disease May Affect Your Health | NHLBI, NIH." Accessed: May 11, 2025. [Online]. Available: https://www.nhlbi.nih.gov/health/sickle-cell-disease/health-effects

[9] E. R. Meier, "Treatment Options for Sickle Cell Disease," *Pediatric Clinics of North America*, vol. 65, no. 3, pp. 427–443, Jun. 2018, doi: 10.1016/j.pcl.2018.01.005.

[10] B. Inusa *et al.*, "Sickle Cell Disease—Genetics, Pathophysiology, Clinical Presentation and Treatment," *IJNS*, vol. 5, no. 2, p. 20, May 2019, doi: 10.3390/ijns5020020.

[11] N. Yasara, A. Premawardhena, and S. Mettananda, "A comprehensive review of hydroxyurea for β-haemoglobinopathies: the role revisited during COVID-19 pandemic," *Orphanet J Rare Dis*, vol. 16, no. 1, p. 114, Dec. 2021, doi: 10.1186/s13023-021-01757-w.

[12] R. N. Paul, O. L. Castro, A. Aggarwal, and P. A. Oneal, "Acute chest syndrome: sickle cell disease: Acute Chest Syndrome," *European Journal of Haematology*, vol. 87, no. 3, pp. 191–207, Sep. 2011, doi: 10.1111/j.1600-0609.2011.01647.x.

[13] J. Crawford, D. Herndon, K. Gmitter, and J. Weiss, "The impact of myelosuppression on quality of life of patients treated with chemotherapy," *Future Oncology*, vol. 20, no. 21, pp. 1515–1530, Jul. 2024, doi: 10.2217/fon-2023-0513.

[14] M. Brito, C. Ginete, A. Ofakunrin, I. Diaku-Akinwumi, and B. P. D. Inusa, "Treating sickle cell disease in resource-limited sub-Saharan Africa: recent strategies and recommendations in addressing the gaps for the provision of evidence-based management," *Expert Review of Hematology*, pp. 1–16, May 2025, doi: 10.1080/17474086.2025.2500599.

[15] K. Khaddour, C. K. Hana, and P. Mewawalla, "Hematopoietic Stem Cell Transplantation," in *StatPearls*, Treasure Island (FL): StatPearls Publishing, 2025. Accessed: May 13, 2025. [Online]. Available: http://www.ncbi.nlm.nih.gov/books/NBK536951/

[16] O. of the Commissioner, "FDA Approves First Gene Therapies to Treat Patients with Sickle Cell Disease," FDA. Accessed: May 13, 2025. [Online]. Available: https://www.fda.gov/news-events/press-announcements/fda-approves-first-gene-therapies-treat-patients-sickle-cell-disease

[17] A. Singh, H. Irfan, E. Fatima, Z. Nazir, A. Verma, and A. Akilimali, "Revolutionary breakthrough: FDA approves CASGEVY, the first CRISPR/Cas9 gene therapy for sickle cell disease," *Annals of Medicine & Surgery*, vol. 86, no. 8, pp. 4555–4559, Aug. 2024, doi: 10.1097/MS9.0000000000002146.

[18] C. T. Quinn, M. C. Paniagua, R. K. DiNello, A. Panchal, and M. Geisberg, "A rapid, inexpensive and disposable point-of-care blood test for sickle cell disease using novel, highly specific monoclonal antibodies," *Br J Haematol*, vol. 175, no. 4, pp. 724–732, Nov. 2016, doi: 10.1111/bjh.14298.

[19] J. Kanter, M. J. Telen, C. Hoppe, C. L. Roberts, J. S. Kim, and X. Yang, "Validation of a novel point of care testing device for sickle cell disease," *BMC Med*, vol. 13, no. 1, p. 225, Dec. 2015, doi: 10.1186/s12916-015-0473-6.

[20] F. B. Piel, S. I. Hay, S. Gupta, D. J. Weatherall, and T. N. Williams, "Global Burden of Sickle Cell Anaemia in Children under Five, 2010–2050: Modelling Based on Demographics, Excess Mortality, and Interventions," *PLoS Med*, vol. 10, no. 7, p. e1001484, Jul. 2013, doi: 10.1371/journal.pmed.1001484.

[21] "Second WHO Model List of Essential In Vitro Diagnostics (2019)." Nov. 20, 2019. https://www.who.int/publications/i/item/WHO-MVP-EMP-2019.05

[22] E. S. Allan L. Louderback, "Hemoglobin Electrophoresis," *Laboratory Procedures: Their Clinical Significance*, 1967.

[23] T. R. Kotila, "GUIDELINES FOR THE DIAGNOSIS OF THE HAEMOGLOBINOPATHIES IN NIGERIA," *Annals of Ibadan Postgraduate Medicine*, vol. Vol.8 No.1, 2010.

[24] J. Old, C. Harteveld, J. Traeger-Synodinos, M. Petrou, M. Angastiniotis, and R. Galanello, *Prevention of Thalassaemias and Other Haemoglobin Disorders: Volume 2: Laboratory Protocols*, 2nd edition. Nicosia (Cyprus), 2012. [Online]. Available: https://www.ncbi.nlm.nih.gov/books/NBK190576/

[25] W. A. Arishi, H. A. Alhadrami, and M. Zourob, "Techniques for the Detection of Sickle Cell Disease: A Review," *Micromachines*, vol. 12, no. 5, p. 519, May 2021, doi: 10.3390/mi12050519.

[26] J. M. Hempe and R. D. Craver, "Separation of hemoglobin variants with similar charge by capillary isoelectric focusing: Value of isoelectric point for identification of common and uncommon hemoglobin variants," *Electrophoresis*, vol. 21, no. 4, pp. 743–748, Mar. 2000, doi: 10.1002/(SICI)1522-2683(20000301)21:4<743::AID-ELPS743>3.0.CO;2-1.

[27] D. Garfin, "Isoelectric focusing," *METHODS IN ENZYMOLOGY*, vol. Vol. 182, pp. 459–477, 1990.

[28] A. Joutovsky, J. Hadzi-Nesic, and M. A. Nardi, "HPLC Retention Time as a Diagnostic Tool for Hemoglobin Variants and Hemoglobinopathies: A Study of 60000 Samples in a Clinical Diagnostic Laboratory," *Clinical Chemistry*, vol. 50, no. 10, pp. 1736–1747, Oct. 2004, doi: 10.1373/clinchem.2004.034991.

[29] M. Bender and K. Carlberg, "Hemoglobin Assays: Advantages and Disadvantages," 2022.

[30] D. Dexter and P. T. McGann, "Saving lives through early diagnosis: the promise and role of point of care testing for sickle cell disease," *Br J Haematol*, vol. 196, no. 1, pp. 63–69, Jan. 2022, doi: 10.1111/bjh.17678.

[31] K. Qua, S. M. Swiatkowski, U. A. Gurkan, and C. M. Pelfrey, "A retrospective case study of successful translational research: Gazelle Hb variant point-of-care diagnostic device for sickle cell disease," *J. Clin. Trans. Sci.*, vol. 5, no. 1, p. e207, 2021, doi: 10.1017/cts.2021.871.

[32] R. An *et al.*, “Multispectral imaging for MicroChip electrophoresis enables point-of-care newborn hemoglobin variant screening,” *Heliyon*, vol. 8, no. 12, p. e11778, Dec. 2022, doi: 10.1016/j.heliyon.2022.e11778.
[33] M. N. Hasan, “Hemechip: An Automated Portable Microchip Electrophoresis Platform for Point-of-Care Sickle Cell Disease Screening”.
[34] S. Fucharoen and D. J. Weatherall, “The Hemoglobin E Thalassemias,” *Cold Spring Harbor Perspectives in Medicine*, vol. 2, no. 8, pp. a011734–a011734, Aug. 2012, doi: 10.1101/cshperspect.a011734.
[35] A. Phasit, S. Panyasai, M. Mayoon, N. Jettawan, and S. Satthakarn, “Phenotypic Expression of Known and Novel Hemoglobin A2-Variants, Hemoglobin A2-Mae Phrik [Delta 52(D3) Asp > Gly, HBD:c.158A > G], Associated with Hemoglobin E [Beta 26(B8) Glu > Lys, HBB:c.79G > A] in Thailand,” *Genes*, vol. 13, no. 6, p. 959, May 2022, doi: 10.3390/genes13060959.
[36] O. Nnodu *et al.*, “HemoTypeSC, a low-cost point-of-care testing device for sickle cell disease: Promises and challenges,” *Blood Cells, Molecules, and Diseases*, vol. 78, pp. 22–28, Sep. 2019, doi: 10.1016/j.bcmd.2019.01.007.
[37] S. R. Mendez-Marti, C. Zik, S. Alan, H. Wang, and W. B. Ershler, “Sickle Cell Screening in Adults: A Current Review of Point-of-Care Testing,” *J Hematol*, vol. 13, no. 3, pp. 53–60, Jun. 2024, doi: 10.14740/jh1272.
[38] M. Stastna, “Continuous flow electrophoretic separation — Recent developments and applications to biological sample analysis,” *Electrophoresis*, vol. 41, no. 1–2, pp. 36–55, Jan. 2020, doi: 10.1002/elps.201900288.
[39] Y. Kang and D. Li, “Electrokinetic motion of particles and cells in microchannels,” *Microfluid Nanofluid*, vol. 6, no. 4, pp. 431–460, Apr. 2009, doi: 10.1007/s10404-009-0408-7.
[40] J. St. L. Philpot, “The use of thin layers in electrophoretic separation,” *Trans. Faraday Soc.*, vol. 35, p. 38, 1940, doi: 10.1039/tf9403500038.
[41] E. L. Durrum, “Continuous Electrophoresis and Ionophoresis on Filter Paper[1],” *J. Am. Chem. Soc.*, vol. 73, no. 10, pp. 4875–4880, Oct. 1951, doi: 10.1021/ja01154a119.
[42] A. X. Apostolopoulos, “Continuous-flow paper electrophoresis in the fractionation of human salivary secretion,” *Archives of Oral Biology*, vol. 12, no. 11, pp. 1275-IN14, Nov. 1967, doi: 10.1016/0003-9969(67)90129-X.
[43] W. G. Glenn and H. A. Jaeger, “An inexpensive continuous paper electrophoresis apparatus,” *J. Chem. Educ.*, vol. 35, no. 7, p. 360, Jul. 1958, doi: 10.1021/ed035p360.
[44] J. H. Lewis, D. Walters, P. Didisheim, and W. R. Merchant, “Application of Continuous Flow Electrophoresis to the Study of the Blood Coagulation Proteins and the Fibrinolytic Enzyme System. I. Normal Human Materials1,” *J. Clin. Invest.*, vol. 37, no. 9, pp. 1323–1331, Sep. 1958, doi: 10.1172/JCI103721.
[45] G. Weber and P. Boček, “Optimized continuous flow electrophoresis,” *Electrophoresis*, vol. 17, no. 12, pp. 1906–1910, Jan. 1996, doi: 10.1002/elps.1150171216.
[46] K. Šlais, “Divergent flow isoelectric focusing,” *Electrophoresis*, vol. 29, no. 12, pp. 2451–2457, Jun. 2008, doi: 10.1002/elps.200700705.
[47] K. Mazanec, J. Bobalova, and K. Šlais, “Divergent flow isoelectric focusing: fast and efficient method for protein sample preparation for mass spectrometry,” *Anal Bioanal Chem*, vol. 393, no. 6–7, pp. 1769–1778, Mar. 2009, doi: 10.1007/s00216-009-2600-8.

[48] M. Stastna and K. Slais, “Preparative divergent flow IEF without carrier ampholytes for separation of complex biological samples,” *Electrophoresis*, vol. 31, no. 3, pp. 433–439, Jan. 2010, doi: 10.1002/elps.200900484.
[49] H. Qiu, K. Obata, K. Tsuburaya, T. Nishimoto, K. Nagato, and K. Takanabe, “Impact of gas bubble slug on high-frequency resistance and cell voltage in water electrolysis device,” *Journal of Power Sources*, vol. 611, p. 234765, Aug. 2024, doi: 10.1016/j.jpowsour.2024.234765.
[50] A. Olanrewaju, M. Beaugrand, M. Yafia, and D. Juncker, “Capillary microfluidics in microchannels: from microfluidic networks to capillaric circuits,” *Lab Chip*, vol. 18, no. 16, pp. 2323–2347, 2018, doi: 10.1039/C8LC00458G.
[51] T. Young, “III. An essay on the cohesion of fluids,” *Phil. Trans. R. Soc.*, vol. 95, pp. 65–87, Dec. 1805, doi: 10.1098/rstl.1805.0005.
[52] N. Gal, D. Lechtman-Goldstein, and D. Weihs, “Particle tracking in living cells: a review of the mean square displacement method and beyond,” *Rheol Acta*, vol. 52, no. 5, pp. 425–443, May 2013, doi: 10.1007/s00397-013-0694-6.
[53] W. Moll and H. Voss, “The diffusion coefficient of haemoglobin,” *Respiration Physiology*, vol. 1, no. 4, pp. 357–365, Jan. 1966, doi: 10.1016/0034-5687(66)90002-8.
[54] G. K. Batchelor, *An Introduction to Fluid Dynamics*, 1st ed. Cambridge University Press, 2000. doi: 10.1017/CBO9780511800955.
[55] N. Nishiyama and T. Yokoyama, “Permeability of porous media: Role of the critical pore size,” *JGR Solid Earth*, vol. 122, no. 9, pp. 6955–6971, Sep. 2017, doi: 10.1002/2016JB013793.
[56] S. Chatterjee, A. Nanda, R. Chowdhury, and P. Bhattacharya, “Mathematical modeling and simulation of solubility and ultrafiltration behavior of hemoglobin in a semi-batch module in the salting-in and -out regions,” *Biochemical Engineering Journal*, vol. 15, no. 1, pp. 11–20, Jul. 2003, doi: 10.1016/S1369-703X(02)00175-4.
[57] “Measuring the surface potential and isoelectric point of glass fibres with a zeta potential analyzer”.
[58] V. S. Stoll and J. S. Blanchard, “[4] Buffers: Principles and practice,” in *Methods in Enzymology*, vol. 182, Elsevier, 1990, pp. 24–38. doi: 10.1016/0076-6879(90)82006-N.
[59] W. J. Ferguson *et al.*, “Hydrogen ion buffers for biological research,” *Analytical Biochemistry*, vol. 104, no. 2, pp. 300–310, May 1980, doi: 10.1016/0003-2697(80)90079-2.
[60] M. Bier, J. Ostrem, and R. B. Marquez, “A new buffering system and its use in electrophoresis and isoelectric focusing,” *Electrophoresis*, vol. 14, no. 1, pp. 1011–1018, Jan. 1993, doi: 10.1002/elps.11501401161.
[61] “Biological Buffers.” Accessed: May 29, 2025. [Online]. Available: http://staff.ustc.edu.cn/~liuyz/methods/buffer.htm
[62] A. Shokrollahi and E. Zare, “Determination of acidity constants of bromophenol blue and phenol red indicators by solution scanometric method and comparison with spectrophotometric results,” *Journal of Molecular Liquids*, vol. 219, pp. 1165–1171, Jul. 2016, doi: 10.1016/j.molliq.2016.01.050.
[63] R. Bhomia, V. Trivedi, N. J. Coleman, and J. C. Mitchell, “The thermal and storage stability of bovine haemoglobin by ultraviolet–visible and circular dichroism spectroscopies,” *Journal of Pharmaceutical Analysis*, vol. 6, no. 4, pp. 242–248, Aug. 2016, doi: 10.1016/j.jpha.2016.02.004.

[64] A. Ashley-Koch, Q. Yang, and R. S. Olney, “Sickle Hemoglobin (Hb S) Allele and Sickle Cell Disease: A HuGE Review,” *American Journal of Epidemiology*, vol. 151, no. 9, pp. 839–845, May 2000, doi: 10.1093/oxfordjournals.aje.a010288.

[65] S. Xie *et al.*, “Carrier ampholyte-free isoelectric focusing on a paper-based analytical device for the fractionation of proteins,” *J of Separation Science*, vol. 41, no. 9, pp. 2085–2091, May 2018, doi: 10.1002/jssc.201701438.

[66] G. Lutišanová, E. Kuzielová, M. T. Palou, and J. Kozánková, “STATIC AND DYNAMIC IN VITRO TEST OF BIOACTIVITY OF GLASS CERAMICS”.

[67] “Lysing red blood cells | UAMS Department of Microbiology and Immunology,” https://medicine.uams.edu/mbim/. Accessed: May 28, 2025. [Online]. Available: https://medicine.uams.edu/mbim/research-cores/flow-cytometry-core-facility/protocols-and-reagents/lysing-red-blood-cells/

[68] C. D. Fitzhugh, M. M. Hsieh, C. D. Bolan, C. Saenz, and J. F. Tisdale, “Granulocyte colony-stimulating factor (G-CSF) administration in individuals with sickle cell disease: time for a moratorium?,” *Cytotherapy*, vol. 11, no. 4, pp. 464–471, Jan. 2009, doi: 10.1080/14653240902849788.

[69] C. T. Quinn and R. E. Ware, “The modern use of hydroxyurea for children with sickle cell anemia,” *haematol*, Jan. 2025, doi: 10.3324/haematol.2023.284633.

[70] Z. Sekyonda, R. An, A. Avanaki, A. Fraiwan, and U. A. Gurkan, “A Novel Approach for Glycosylated Hemoglobin Testing Using Microchip Affinity Electrophoresis,” *IEEE Trans. Biomed. Eng.*, vol. 70, no. 5, pp. 1473–1480, May 2023, doi: 10.1109/TBME.2022.3218501.

[71] E. C. Kline, R. Duong, Q. Wang, and B. R. Lutz, “Simplified MS2 phage-like particle production including a novel maturation protein internal fusion affinity tag,” *Biotechnology & Biotechnological Equipment*, vol. 39, no. 1, p. 2457691, Dec. 2025, doi: 10.1080/13102818.2025.2457691.

[72] T. A. Kunkel, “Rapid and efficient site-specific mutagenesis without phenotypic selection.,” *Proc. Natl. Acad. Sci. U.S.A.*, vol. 82, no. 2, pp. 488–492, Jan. 1985, doi: 10.1073/pnas.82.2.488.

[73] “Q5® Site-Directed Mutagenesis (E0554) v1,” Nov. 07, 2014. doi: 10.17504/protocols.io.cjpumm.

[74] Leo. Brewer, “Thermodynamic Properties of the Oxides and their Vaporization Processes.,” *Chem. Rev.*, vol. 52, no. 1, pp. 1–75, Feb. 1953, doi: 10.1021/cr60161a001.

[75] Y. Qin, X. Ouyang, Y. Lv, W. Liu, Q. Liu, and S. Wang, “A Review of Carbon-Based Conductive Inks and Their Printing Technologies for Integrated Circuits,” *Coatings*, vol. 13, no. 10, p. 1769, Oct. 2023, doi: 10.3390/coatings13101769.